

Gauge dependence of on-shell and pole mass renormalization prescriptions

Yong Zhou

*Beijing University of Posts and Telecommunications,
school of science P.O. Box 123, Beijing 100876, China*

We discuss the gauge dependence of physical parameter's definitions under the on-shell and pole mass renormalization prescriptions. By two-loop-level calculations we prove for the first time that the on-shell mass renormalization prescription makes physical result gauge dependent. On the other hand, such gauge dependence doesn't appear in the result of the pole mass renormalization prescription. Our calculation also implies the difference of the physical results between the two mass renormalization prescriptions cannot be neglected at two-loop level.

PACS numbers: 11.10.Gh, 12.15.Lk

I. INTRODUCTION

The conventional on-shell mass renormalization prescription has been present for a long time. It renormalizes the real part of particle's inverse propagator to zero at physical mass point. For boson the on-shell mass renormalization condition is [1, 2]

$$m^2 - m_0^2 + \text{Re}\Sigma(m^2) = 0, \quad (1)$$

where m_0 is the bare mass and Σ is the boson's diagonal self energy (for vector boson it is the transverse diagonal self energy). But recently people proposed a new mass renormalization prescription which renormalizes both the real and the imaginary parts of the particle's inverse propagator to zero at the (complex) pole of the particle's propagator, i.e. [3, 4]

$$\bar{s} - m_0^2 + \Sigma(\bar{s}) = 0, \quad (2)$$

where \bar{s} is the pole of the particle's propagator. Written $\bar{s} = m_2^2 - im_2\Gamma_2$, m_2 is defined as the physical mass of the particle [3]. Putting the expression of \bar{s} into Eq.(2) one has [3, 4]

$$m_2^2 - m_0^2 + \text{Re}\Sigma(\bar{s}) = 0, \quad m_2\Gamma_2 = \text{Im}\Sigma(\bar{s}). \quad (3)$$

By expanding Eqs.(3) at $\bar{s} = m_2^2$ one readily has (see Eq.(1)) [3, 4]

$$m - m_2 = \Gamma_2 \text{Im}\Sigma'(m_2^2)/2 + O(g^6), \quad (4)$$

where $\Sigma'(m_2^2) = \partial\Sigma(m_2^2)/\partial p^2$ and g is a generic coupling constant. For unstable boson the r.h.s. of Eq.(4) is gauge dependent [3, 4]. So A. Sirlin et al. claim that the on-shell mass definition m of unstable particles is gauge dependent, since the pole mass definition m_2 is gauge independent [3, 4, 5, 6].

But the conclusion that the pole mass definition m_2 is gauge independent has been proposed for not very long time. We still need to search new and stricter proofs to prove this conclusion. In this paper we will discuss if the pole mass definition is gauge independent and investigate the difference of physical result between the on-shell and pole mass renormalization prescriptions. The arrangement of this paper is as follows: firstly we discuss the gauge dependencies of the counterterms of gauge boson W and Z's mass and the sine of the weak mixing angle under the on-shell and pole mass renormalization prescriptions; then we discuss the gauge dependence of the two-loop-level cross section of the physical process $\mu \rightarrow \nu_\mu e^- \bar{\nu}_e$ under the two mass renormalization prescriptions; Lastly we give the conclusion.

II. GAUGE DEPENDENCIES OF PHYSICAL PARAMETER'S COUNTERTERMS UNDER THE ON-SHELL AND POLE MASS RENORMALIZATION PRESCRIPTIONS

The gauge invariance of Lagrangian always requires the bare physical parameters are gauge independent. The natural deduction of this conclusion is the counterterms of physical parameters should also be gauge independent [7], since the bare physical parameter can be divided into physical parameter and the corresponding counterterm, and the physical parameter is of course gauge independent. This criterion could be used to judge which mass renormalization prescription is reasonable, in other words which mass definition is gauge independent. In the following we will discuss the gauge dependence of the counterterms of gauge boson W and Z's mass and the sine of the weak mixing angle under the on-shell and pole mass renormalization prescriptions. For convenience we only discuss the dependence of W gauge parameter ξ_W in the R_ξ gauge, and we only introduce physical parameter's counterterms (i.e. we don't introduce field renormalization constants). The computer program packages *FeynArts* and *FeynCalc* [8] have been used in the following calculations. Here we note there are some early two-loop-level calculations about the massive gauge boson's self energies in Ref.[9].

From Eqs.(1,3) one has for massive gauge boson [10]

$$\begin{aligned}\delta m^2 &= Re\Sigma^T(m^2), \\ \delta m_2^2 &= Re\Sigma^T(m_2^2) + m_2\Gamma_2 Im\Sigma^T(m_2^2) + O(g^6),\end{aligned}\tag{5}$$

where Σ^T denotes the transverse self energy of the gauge boson. The one-loop-level mass counterterms of W and Z have been proven gauge independent [6]. So we only need to discuss the two-loop-level case. Firstly m and m_2 should be regarded as equal quantities, since both of them are regarded as the physical mass of the same particle. Therefore we find the two-loop-level difference of the two mass counterterm is $m\Gamma Im\Sigma^T(m^2)$. Every part of this term contains gauge-parameter-dependent Heaviside functions (which come from the one-loop-level $Im\Sigma^T$ [3, 4]). So in order to discuss the difference of the gauge dependence of the two mass counterterms we only need to calculate the gauge dependence of the singularities of the two-loop-level $Re\Sigma^T(m^2)$, because only the singularities of $Re\Sigma^T(m^2)$ in $Re\Sigma^T(m^2)$ contain Heaviside functions. In other words for our purpose we only need to discuss the gauge dependence of the part which contains Heaviside functions of the two mass counterterms.

The two-loop-level self energies can be classified into two kinds: one kind contains one-loop-level counterterms, the other kind doesn't contain any counterterm. Since except for CKM matrix elements [11] all of the one-loop-level counterterms of physical parameters are real numbers and don't contain Heaviside function [2], the first kind self energy doesn't contribute to the singularities of the real part of the self energy, because except the one-loop-level counterterm the left part of this kind self energy is an one-loop-level self energy which real part doesn't contain singularities. Here we don't need to worry about the problem that the CKM matrix elements and their counterterms are complex numbers, because the total contribution of them to the real part of the gauge boson's self energy is real number (the correctness of this conclusion can be see from the following calculations). So we only need to calculate the contributions of the second kind self energy.

According to the *cutting rules* [12] the second kind self energy can be classified into three kinds: one kind doesn't contain singularity, the second kind contains singularities, but its singularities don't contribute to the real part of the self energy, the third kind contains singularities and its singularities contribute to the real part of the self energy. The topologies of the three kind self energies are shown in Fig.1, Fig.2 and Fig.3. Here we note the middle propagator (denoted by broken line) in the one-particle-reducible diagrams of Fig.(1-3) is different from the external-line particles. The tadpole diagrams are also included in Fig.(1-3), because we don't introduce the tadpole counterterm [6].

Obviously we only need to calculate the contribution of the singularities of Fig.3 to the real part of the gauge boson's self energy. In Fig.3 we also draw the possible cuts/singularities of the first four topologies which contribute to the real part of the gauge boson's self energy (the arrow on the inner line denotes the corresponding propagator is cut [12]). The possible cuts of the left

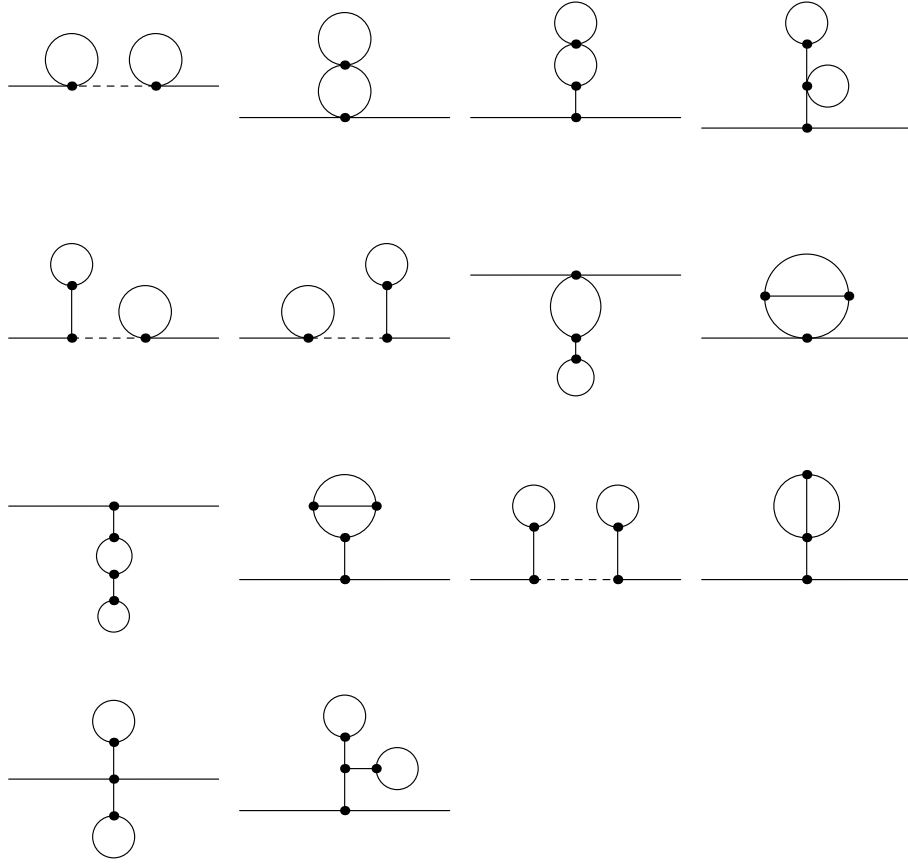


FIG. 1: Topologies of the two-loop-level self energy which lacks counterterm and singularity.

two topologies which contribute to the real part of the gauge boson's self energy are shown in Fig.4 and Fig.5.

A. Gauge dependence of W mass counterterm under the two mass renormalization prescriptions

In the standard model of particle physics the first topology of Fig.3 doesn't contribute to W transverse self energy, so we don't need to calculate its contribution. For the second topology of Fig.3 there are 39 Feynman diagrams in the standard model, but none of them satisfies the corresponding cutting condition. The case of the third topology of Fig.3 is same as the case of the second topology. For the 4th topology of Fig.3 there are two W self energy diagrams as shown in Fig.6 which satisfy the corresponding cutting condition. Using the cutting rules we obtain the gauge-parameter-dependent contribution of the cuts of Fig.6 to the real part of W transverse self

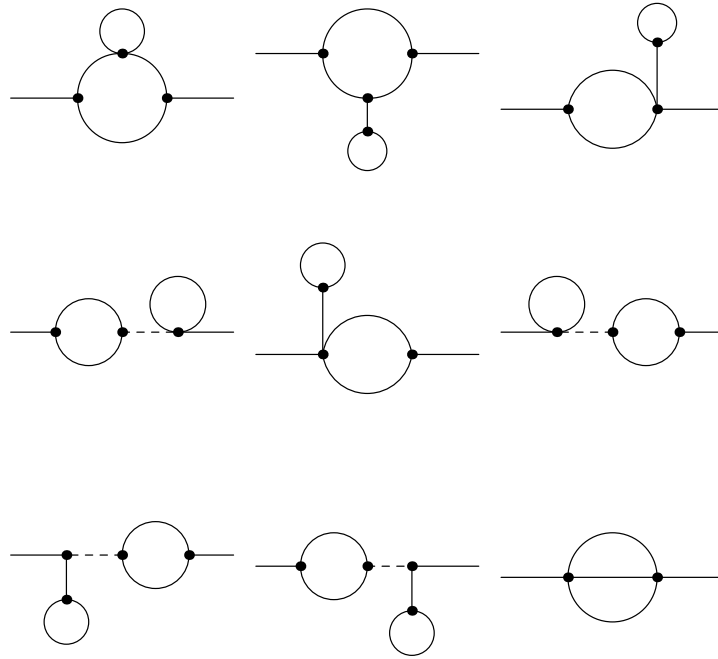


FIG. 2: Topologies of the two-loop-level self energy which lacks counterterm and its singularities don't contribute to the real part of the self energy.

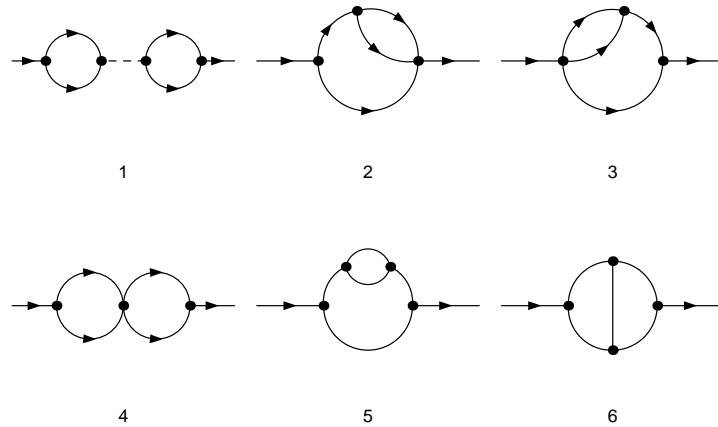


FIG. 3: Topologies of the two-loop-level self energy which lacks counterterm and its singularities contribute to the real part of the self energy.

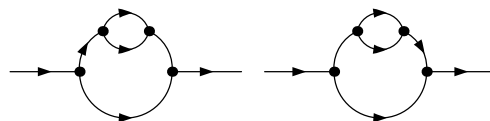


FIG. 4: Possible cuts of the 5th topology of Fig.3 which contribute to the real part of the self energy.

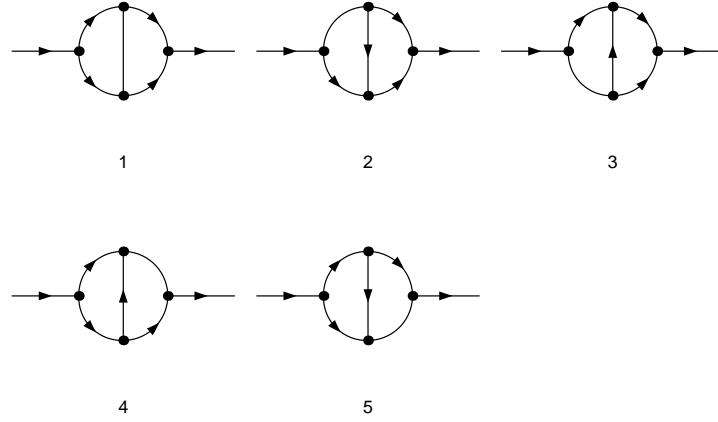


FIG. 5: Possible cuts of the 6th topology of Fig.3 which contribute to the real part of the self energy.

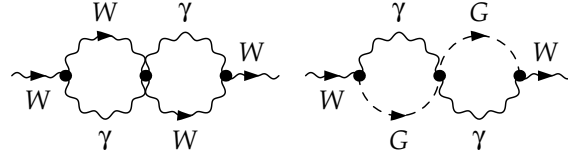


FIG. 6: W self energy diagrams which satisfy the 4th topology of Fig.3 and the corresponding cutting condition.

energy:

$$Re\Sigma_{WW}^T(m_W^2)|_{\xi_W-cut} = \frac{\alpha^2 m_W^2}{4608} (1 - \xi_W)^3 (\xi_W^5 - 3\xi_W^4 - 6\xi_W^3 - 46\xi_W^2 + 165\xi_W + 465) \theta[1 - \xi_W], \quad (6)$$

where Σ_{WW}^T is W transverse self energy, m_W and ξ_W is W's mass and gauge parameter, α is the fine structure constant, θ is the Heaviside function, and the subscript ξ_W-cut denotes the ξ_W -dependent contribution from the cuts/singularities. In the follows we restrict ourselves to $\xi_W > 0$ [4].

For the 5th topology of Fig.3 there are 14 W's self energy diagrams as shown in Fig.7 which are ξ_W -dependent and satisfy the cutting conditions of Fig.4. After careful calculations we obtain the gauge-parameter-dependent contribution of the cuts of Fig.7 to the real part of W transverse self energy:

$$\begin{aligned} Re\Sigma_{WW}^T(m_W^2)|_{\xi_W-cut} = & \frac{\alpha^2 m_W^2}{128s_w^4} \left[\sum_{i=e,\mu,\tau} \frac{1}{x_i} (1 - x_i) (x_i - \xi_W)^2 (x_i^2 + x_i - 2) \theta[m_i - \sqrt{\xi_W} m_W] \right. \\ & + \frac{1}{\xi_W^2} s_w^2 (1 - \xi_W)^3 \sum_{i=e,\mu,\tau} x_i (x_i - \xi_W)^2 \theta[\sqrt{\xi_W} m_W - m_i] \theta[1 - \xi_W] \\ & \left. + 3 \sum_{i=u,c} \sum_{j=d,s,b} \frac{1}{x_i} |V_{ij}|^2 (\xi_W - x_i + x_j) A_{ij} B_{ij} C_{ij} \theta[m_i - m_j - \sqrt{\xi_W} m_W] \right] \end{aligned}$$

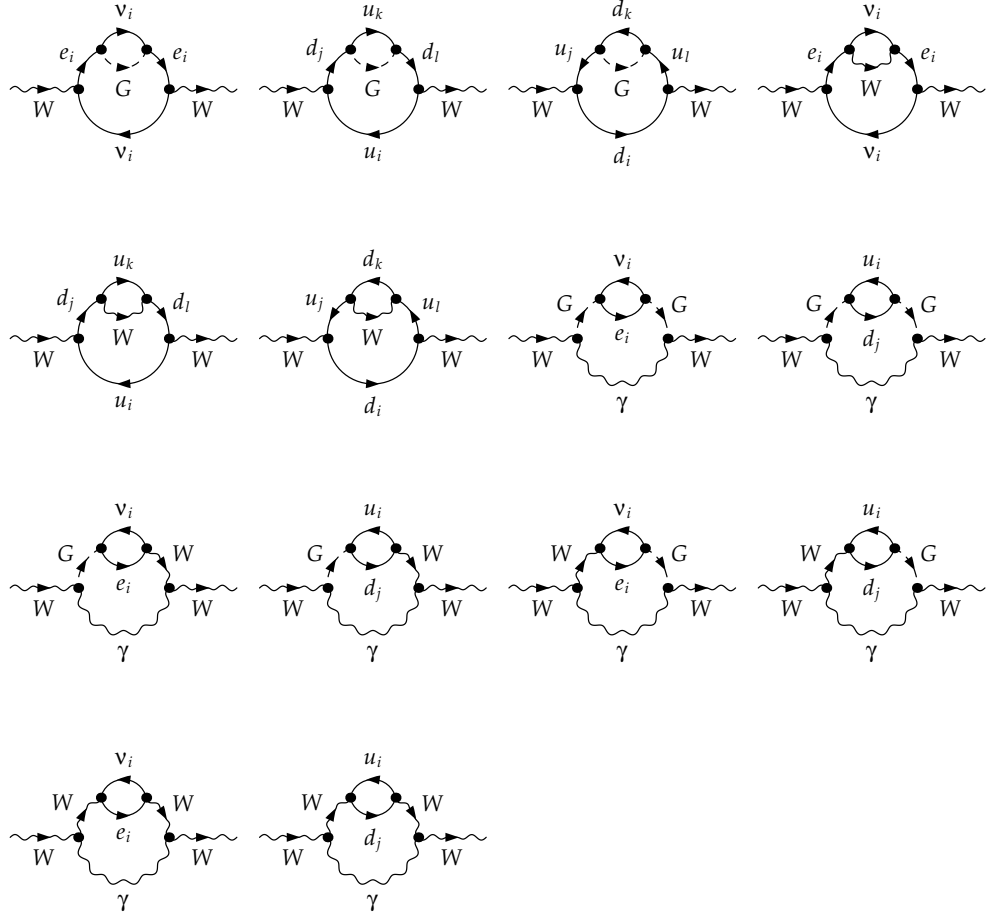


FIG. 7: ξ_W -dependent W self energy diagrams which satisfy the 5th topology of Fig.3 and the cutting conditions of Fig.4.

$$\begin{aligned}
& + 3 \sum_{i=u,c} \sum_{j=d,s,b} \frac{1}{x_j} |V_{ij}|^2 (\xi_W - x_j + x_i) A_{ij} B_{ij} C_{ij} \theta[m_j - m_i - \sqrt{\xi_W} m_W] \\
& + \frac{3}{\xi_W^2} s_w^2 (1 - \xi_W)^3 \sum_{i=u,c} \sum_{j=d,s,b} |V_{ij}|^2 (\xi_W (x_i + x_j) - (x_i - x_j)^2) C_{ij} \\
& \times \theta[\sqrt{\xi_W} m_W - m_i - m_j] \theta[1 - \xi_W] \Big] ,
\end{aligned} \tag{7}$$

where s_w is the sine of the weak mixing angle, $x_i = m_i^2/m_W^2$, $x_j = m_j^2/m_W^2$, V_{ij} is the CKM matrix element [11], and

$$\begin{aligned}
A_{ij} &= \sqrt{(x_i - x_j)^2 - 2(x_i + x_j) + 1}, \\
B_{ij} &= 2 - (x_i + x_j) - (x_i - x_j)^2, \\
C_{ij} &= \sqrt{(x_i - x_j)^2 - 2\xi_W (x_i + x_j) + \xi_W^2}.
\end{aligned} \tag{8}$$

For the 6th topology of Fig.3 there are 53 W self energy diagrams as shown in Fig.8 which are

ξ_W -dependent and satisfy the cutting conditions of Fig.5. We will calculate the contributions of the five cuts of Fig.5 one by one. Firstly we obtain the gauge-parameter-dependent contribution of the first cut of Fig.5 to the real part of W transverse self energy:

$$\begin{aligned} Re\Sigma_{WW}^T(m_W^2)|_{\xi_W-cut} = & -\frac{\alpha^2 m_W^2}{576s_w^2} \left[3 \sum_{i=u,c} \sum_{j=d,s,b} |V_{ij}|^2 A_{ij} B_{ij} + \sum_{i=e,\mu,\tau} (1-x_i)^2 (2+x_i) \right] \\ & \times (1-\xi_W)(\xi_W^2 - 2\xi_W - 11) \theta[1-\xi_W] - \frac{\alpha^2 m_W^2}{4608} (1-\xi_W)^3 \\ & \times (\xi_W^5 - 3\xi_W^4 - 6\xi_W^3 - 46\xi_W^2 + 165\xi_W + 465) \theta[1-\xi_W]. \end{aligned} \quad (9)$$

Then we obtain the gauge-parameter-dependent contributions of the second and third cuts of Fig.5 to the real part of W transverse self energy:

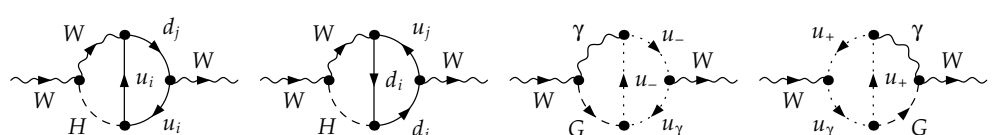
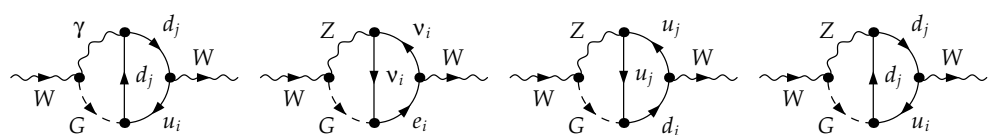
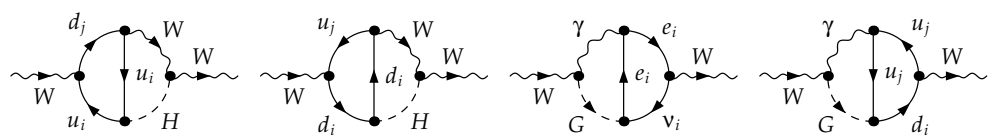
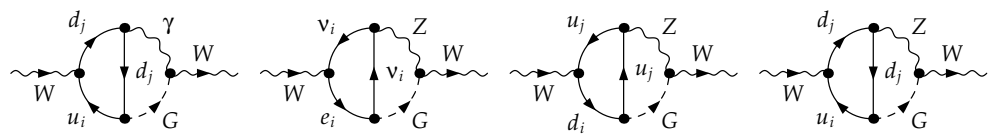
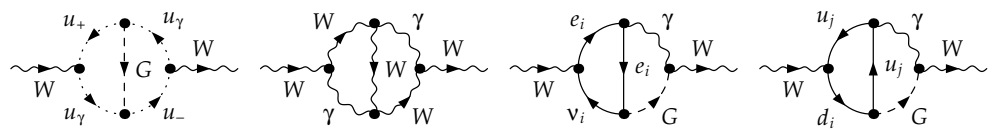
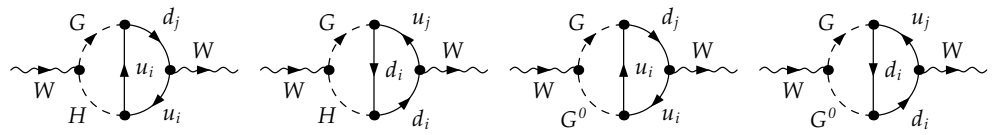
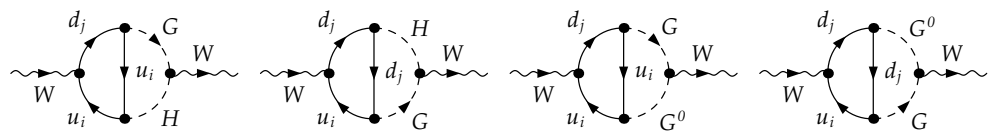
$$\begin{aligned} Re\Sigma_{WW}^T(m_W^2)|_{\xi_W-cut} = & -\frac{\alpha^2 m_W^2}{256s_w^4} \left[\sum_{i=e,\mu,\tau} \frac{1}{x_i} (1-x_i)(x_i-\xi_W)^2 (x_i^2 + x_i - 2) \theta[m_i - \sqrt{\xi_W} m_W] \right. \\ & + \frac{1}{\xi_W^2} s_w^2 (1-\xi_W)^3 \sum_{i=e,\mu,\tau} x_i (x_i - \xi_W)^2 \theta[\sqrt{\xi_W} m_W - m_i] \theta[1-\xi_W] \\ & + 3 \sum_{i=u,c} \sum_{j=d,s,b} \frac{1}{x_i} |V_{ij}|^2 (\xi_W - x_i + x_j) A_{ij} B_{ij} C_{ij} \theta[m_i - m_j - \sqrt{\xi_W} m_W] \\ & + 3 \sum_{i=u,c} \sum_{j=d,s,b} \frac{1}{x_j} |V_{ij}|^2 (\xi_W - x_j + x_i) A_{ij} B_{ij} C_{ij} \theta[m_j - m_i - \sqrt{\xi_W} m_W] \\ & + \frac{3}{\xi_W^2} s_w^2 (1-\xi_W)^3 \sum_{i=u,c} \sum_{j=d,s,b} |V_{ij}|^2 (\xi_W(x_i + x_j) - (x_i - x_j)^2) C_{ij} \\ & \left. \times \theta[\sqrt{\xi_W} m_W - m_i - m_j] \theta[1-\xi_W] \right]. \end{aligned} \quad (10)$$

Lastly we find the gauge-parameter-dependent contributions of the 4th and 5th cuts of Fig.5 to the real part of W transverse self energy are same as those of the second and the third cuts of Fig.5 (this point can be seen from the symmetries of the four cuts).

Summing up all of the above results we obtain the gauge dependence of the singularities of the real part of W two-loop-level transverse self energy (see Eqs.(6,7,9,10) and the corresponding discussions)

$$\begin{aligned} Re\Sigma_{WW}^T(m_W^2)|_{\xi_W-cut} = & -\frac{\alpha^2 m_W^2}{576s_w^2} \left[3 \sum_{i=u,c} \sum_{j=d,s,b} |V_{ij}|^2 A_{ij} B_{ij} + \sum_{i=e,\mu,\tau} (1-x_i)^2 (2+x_i) \right] \\ & \times (1-\xi_W)(\xi_W^2 - 2\xi_W - 11) \theta[1-\xi_W]. \end{aligned} \quad (11)$$

From Eq.(5) one finds Eq.(11) is just the gauge dependence of the part containing Heaviside functions of W mass counterterm under the on-shell mass renormalization prescription. So Eq.(11) proves the W mass counterterm of on-shell mass renormalization prescription is gauge dependent.



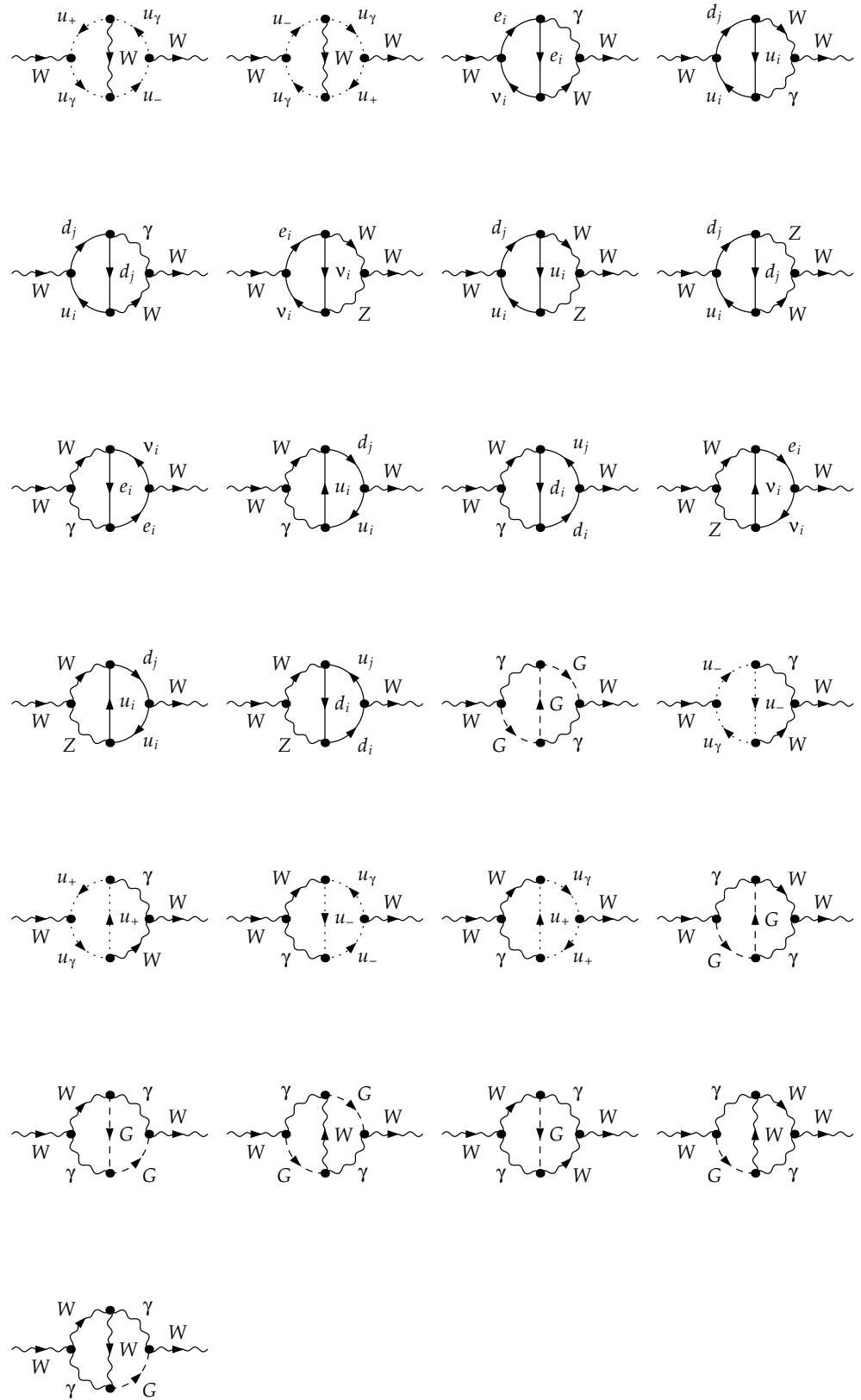


FIG. 8: ξ_W -dependent W self energy diagrams which satisfy the 6th topology of Fig.3 and the cutting conditions of Fig.5.

In order to discuss the gauge dependence of W mass counterterm of the pole mass renormalization prescription we calculate the term (see Eq.(5))

$$m_W \Gamma_W \operatorname{Im} \Sigma_{WW}^{T'}(m_W^2)|_{\xi_W - \text{cut}} = \frac{\alpha^2 m_W^2}{576 s_w^2} \left[3 \sum_{i=u,c} \sum_{j=d,s,b} |V_{ij}|^2 A_{ij} B_{ij} + \sum_{i=e,\mu,\tau} (1-x_i)^2 (2+x_i) \right] \times (1-\xi_W)(\xi_W^2 - 2\xi_W - 11) \theta[1-\xi_W]. \quad (12)$$

Combining Eq.(11) and Eq.(12) one gets (see Eq.(5))

$$\delta m_W^2|_{\xi_W - \text{cut}} = 0 \quad \text{under pole mass renormalization prescription.} \quad (13)$$

This result indicates the part containing Heaviside functions of W mass counterterm of the pole mass renormalization prescription is gauge independent.

B. Gauge dependence of Z mass counterterm under the two mass renormalization prescriptions

Similarly as the case of W gauge boson We only calculate the gauge dependence of the part containing Heaviside function of the real part of Z two-loop-level transverse self energy. The topologies of Z two-loop-level self energy needing calculated have been shown in Fig.3.

For the first topology of Fig.3 only the diagram whose middle propagator (denoted by the broken line) is photon contributes to Z transverse self energy. After careful calculation we obtain the ξ_W -dependent contribution of the cut of the first topology of Fig.3 to the real part of Z transverse self energy

$$\begin{aligned} & \operatorname{Re} \Sigma_{ZZ}^T(m_Z^2)|_{\xi_W - \text{cut}} \\ = & \frac{\alpha^2 m_Z^2}{6912 c_w^6 s_w^2} (1-4c_w^2 \xi_W)^{3/2} \left[\frac{3}{c_w^2} (1-4c_w^2 \xi_W)^{3/2} + 8(3(4c_w^2 - 3) \sum_{i=e,\mu,\tau} + 2(8c_w^2 - 5) \sum_{i=u,c} \right. \\ & + (4c_w^2 - 1) \sum_{i=d,s,b}) \sqrt{1-4c_w^2 x_i} (2c_w^2 x_i + 1) \left. \right] \theta \left[\frac{1}{c_w} - 2\sqrt{\xi_W} \right] + \frac{\alpha^2 m_Z^2}{1728 c_w^6} D E \\ & \times \left[\frac{3 s_w^2}{c_w^2} D E - \frac{3}{c_w^2} (1-4c_w^2 \xi_W)^{3/2} - 4(3(4c_w^2 - 3) \sum_{i=e,\mu,\tau} + 2(8c_w^2 - 5) \sum_{i=u,c} + (4c_w^2 - 1) \sum_{i=d,s,b}) \right. \\ & \times \left. \sqrt{1-4c_w^2 x_i} (2c_w^2 x_i + 1) \right] \theta \left[\frac{1}{c_w} - \sqrt{\xi_W} - 1 \right], \end{aligned} \quad (14)$$

where m_Z is Z mass, c_w is the cosine of the weak mixing angle, and

$$\begin{aligned} D &= \sqrt{(\xi_W - 1)^2 c_w^4 - 2(\xi_W + 1)c_w^2 + 1}, \\ E &= (\xi_W - 1)^2 c_w^4 - 2(\xi_W - 5)c_w^2 + 1. \end{aligned} \quad (15)$$

For the second topology of Fig.3 there are four Z self-energy diagrams as shown in Fig.9 which satisfy the corresponding cutting condition. By the cutting rules we obtain the ξ_W -dependent

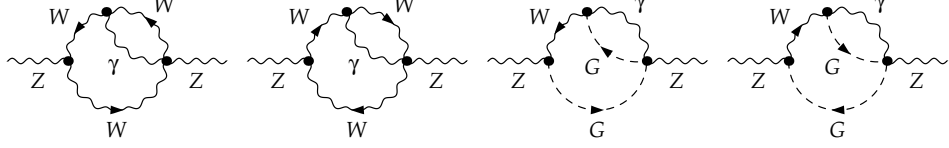


FIG. 9: Z self-energy diagrams which satisfy the second topology of Fig.3 and the corresponding cutting condition.

contribution of the cuts of Fig.9 to the real part of Z transverse self energy :

$$\begin{aligned}
 Re\Sigma_{ZZ}^T(m_Z^2)|_{\xi_W-cut} = & \frac{\alpha^2 m_W^2}{1536 c_w^4} (\xi_W - 1) D [(\xi_W - 1)^3 (\xi_W^3 - \xi_W^2 - 3\xi_W - 33) c_w^6 \\
 & - (\xi_W - 1)(3\xi_W^4 - 9\xi_W^3 - 29\xi_W^2 + 101\xi_W + 366) c_w^4 \\
 & + (3\xi_W^4 - 10\xi_W^3 - 22\xi_W^2 + 170\xi_W - 93) c_w^2 - \xi_W^3 \\
 & + 2\xi_W^2 + 5\xi_W - 18] \theta \left[\frac{1}{c_w} - \sqrt{\xi_W} - 1 \right]. \tag{16}
 \end{aligned}$$

For the third topology of Fig.3 there are also four Z self-energy diagrams as shown in Fig.10 which satisfy the corresponding cutting condition. Obviously Fig.9 and Fig.10 are right-and-left

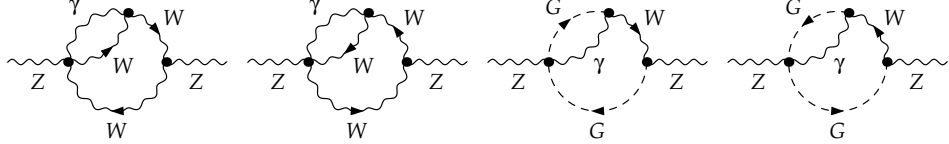


FIG. 10: Z self-energy diagrams which satisfy the third topology of Fig.3 and the corresponding cutting condition.

symmetric. Through calculations we find the ξ_W -dependent contribution of the cuts of Fig.10 to the real part of Z transverse self energy is just equal to that of Fig.9.

For the 4th topology of Fig.3 there are six Z self-energy diagrams as shown in Fig.11 which satisfy the corresponding cutting rules. After careful calculations we obtain the ξ_W -dependent contribution of the cuts of Fig.11 to the real part of Z transverse self energy:

$$\begin{aligned}
 Re\Sigma_{ZZ}^T(m_Z^2)|_{\xi_W-cut} = & \frac{\alpha^2 m_W^2}{4608 c_w^8 s_w^4} (1 - 4 c_w^2 \xi_W)^3 (2c_w^6 - 4c_w^4 + 2c_w^2 - 3) \theta \left[\frac{1}{c_w} - 2\sqrt{\xi_W} \right] \\
 & + \frac{\alpha^2 m_W^2}{2304 c_w^8} [(\xi_W - 1)^6 c_w^{14} - 6(\xi_W - 1)^4 (\xi_W^2 + 11\xi_W + 22) c_w^{12} \\
 & + 3(\xi_W - 1)^2 (12\xi_W^3 + 65\xi_W^2 + 10\xi_W + 201) c_w^{10}
 \end{aligned}$$

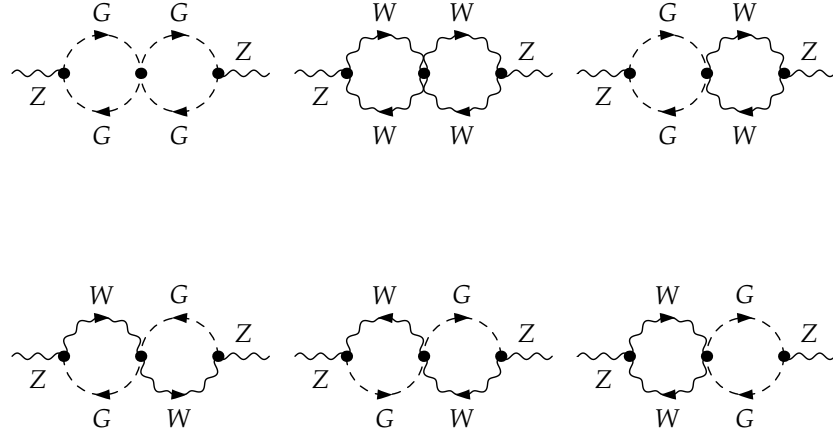
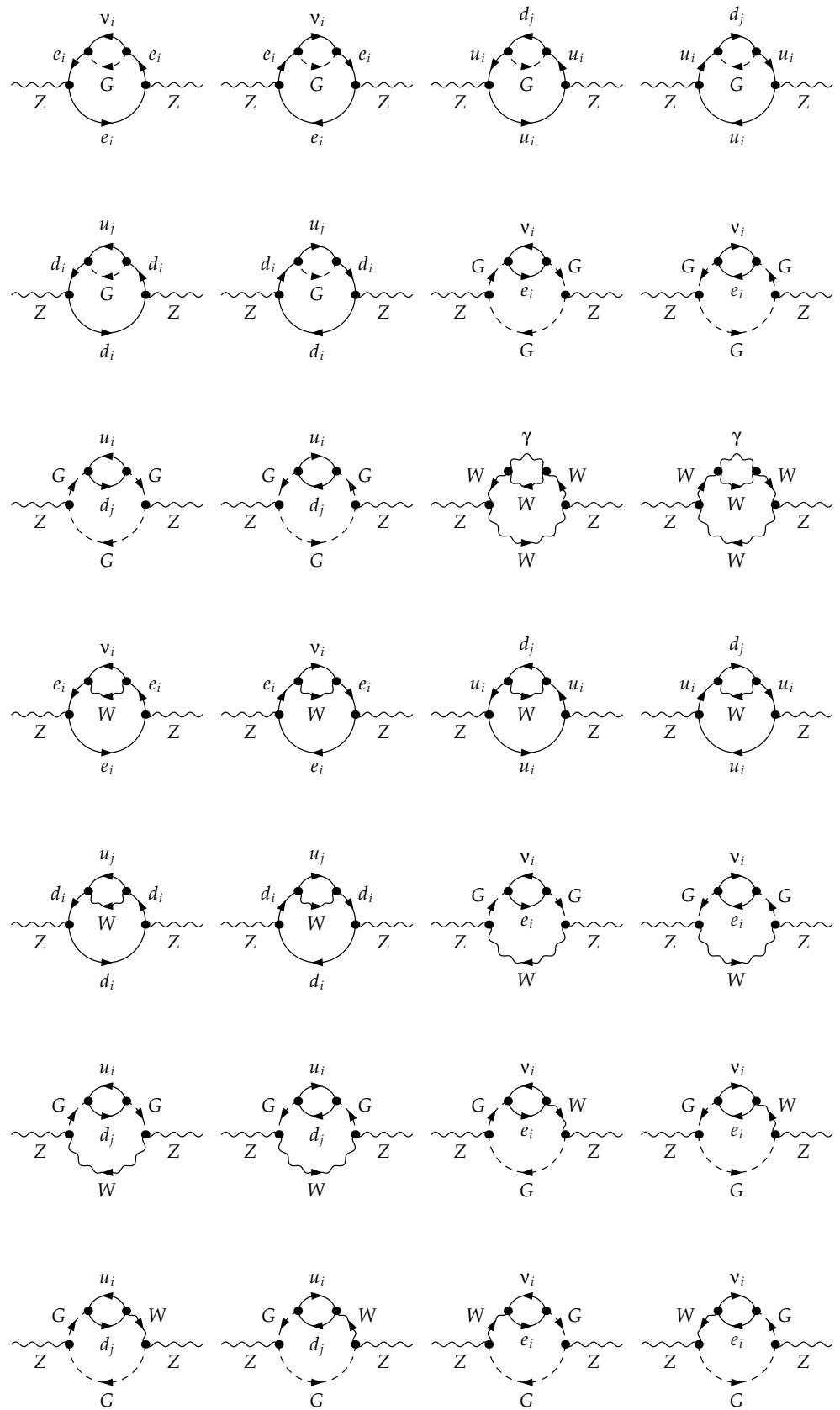


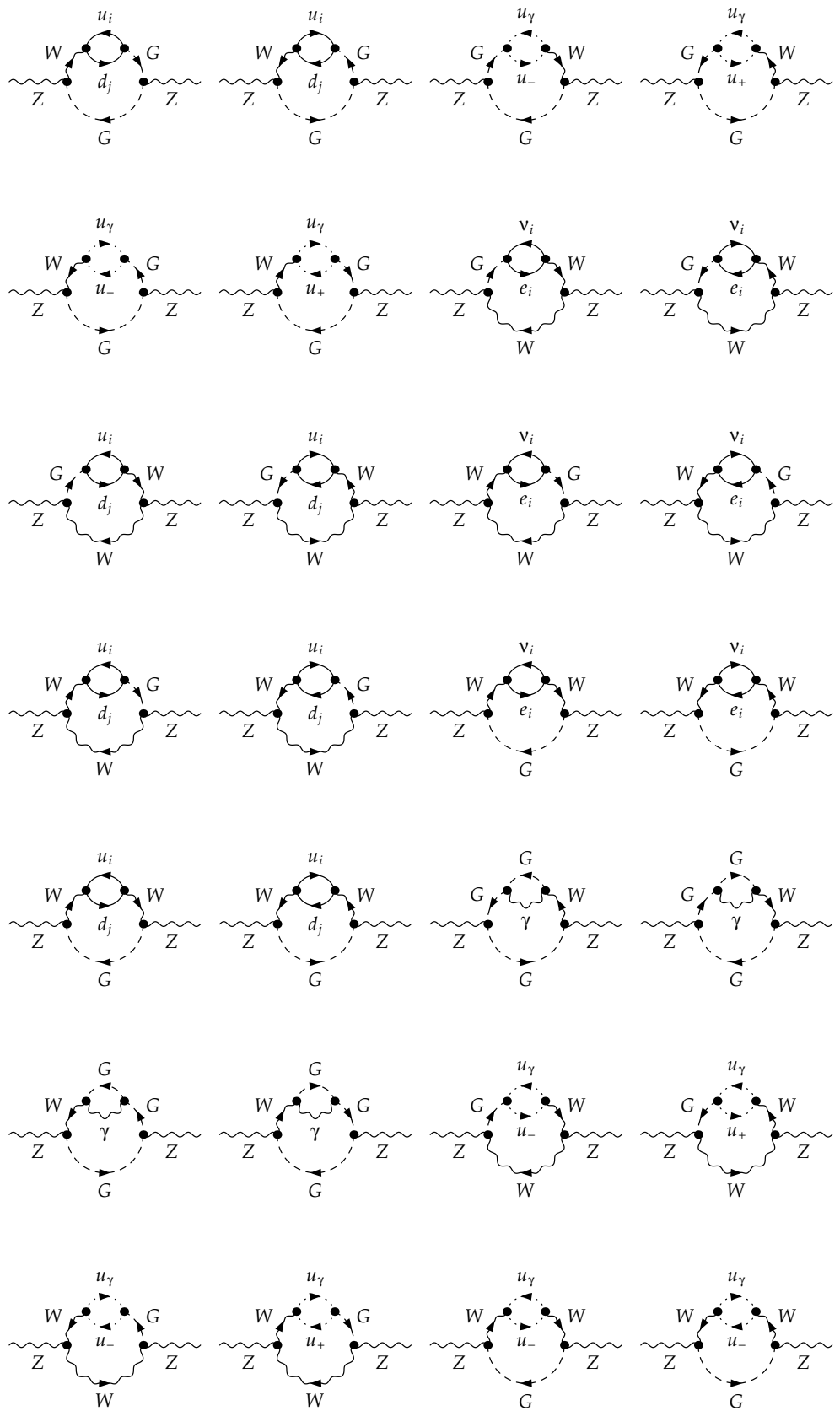
FIG. 11: Z self-energy diagrams which satisfy the 4th topology of Fig.3 and the corresponding cutting condition.

$$\begin{aligned}
& - 2(45\xi_W^4 + 46\xi_W^3 - 228\xi_W^2 - 150\xi_W + 415)c_w^8 \\
& + 3(40\xi_W^3 - 19\xi_W^2 - 98\xi_W + 109)c_w^6 - 6(15\xi_W^2 - 17\xi_W - 12)c_w^4 \\
& + (36\xi_W - 35)c_w^2 - 6] \theta\left[\frac{1}{c_w} - \sqrt{\xi_W} - 1\right] - \frac{\alpha^2 m_W^2}{1152 c_w^8 s_w^2} D \sqrt{1 - 4 c_w^2 \xi_W} \\
& \times [4(\xi_W - 1)^2 \xi_W c_w^{10} - (4\xi_w^3 + \xi_W^2 - 38\xi_W + 1)c_w^8 \\
& + 3(4\xi_W^3 + 19\xi_W^2 - 32\xi_W - 3)c_w^6 - 3(9\xi_W^2 - 10\xi_W - 8)c_w^4 \\
& + (18\xi_W - 11)c_w^2 - 3] \theta\left[\frac{1}{c_w} - \sqrt{\xi_W} - 1\right]. \tag{17}
\end{aligned}$$

For the 5th topology of Fig.3 there are 84 Z self-energy diagrams as shown in Fig.12 which satisfy the cutting conditions of Fig.4. After careful calculations we obtain the ξ_W -dependent contribution of the cuts of Fig.12 to the real part of Z transverse self energy:

$$\begin{aligned}
& \text{Re}\Sigma_{ZZ}^T(m_Z^2)|_{\xi_W-\text{cut}} \\
& = \frac{\alpha^2 m_W^2}{192 c_w^2 s_w^2} D E \left[\sum_{i=e,\mu,\tau} (1-x_i)^2 (2+x_i) + 3 \sum_{i=u,c} \sum_{j=d,s,b} |V_{ij}|^2 A_{ij} B_{ij} \right] \theta\left[\frac{1}{c_w} - \sqrt{\xi_W} - 1\right] \\
& + \frac{\alpha^2 m_W^2}{64 s_w^4 \xi_W^2} (1 - 4 c_w^2 \xi_W)^{3/2} \sum_{i=e,\mu,\tau} x_i (x_i - \xi_W)^2 \theta\left[\frac{1}{c_w} - 2\sqrt{\xi_W}\right] \theta[\sqrt{\xi_W} m_W - m_i] \\
& + \frac{3 \alpha^2 m_W^2}{64 s_w^4 \xi_W^2} (1 - 4 c_w^2 \xi_W)^{3/2} \sum_{i=u,c} \sum_{j=d,s,b} |V_{ij}|^2 C_{ij} (\xi_W (x_i + x_j) - (x_i - x_j)^2) \\
& \times \theta\left[\frac{1}{c_w} - 2\sqrt{\xi_W}\right] \theta[\sqrt{\xi_W} m_W - m_i - m_j] - \frac{\alpha^2 m_W^2}{64 c_w^4 s_w^4} (2 c_W^2 - 1) \sum_{i=e,\mu,\tau} \frac{1}{x_i} \sqrt{1 - 4 c_w^2 x_i} \\
& \times (x_i - \xi_W)^2 (2 c_w^2 - 1 + c_w^2 (4 c_w^2 - 5) x_i) \theta[m_i - \sqrt{\xi_W} m_W] \\
& + \frac{\alpha^2 m_W^2}{192 c_w^4 s_w^4} (4 c_W^2 - 1) \sum_{i=u,c} \sum_{j=d,s,b} \frac{1}{x_i} |V_{ij}|^2 C_{ij} \sqrt{1 - 4 c_w^2 x_i} (\xi_W - x_i + x_j)
\end{aligned}$$





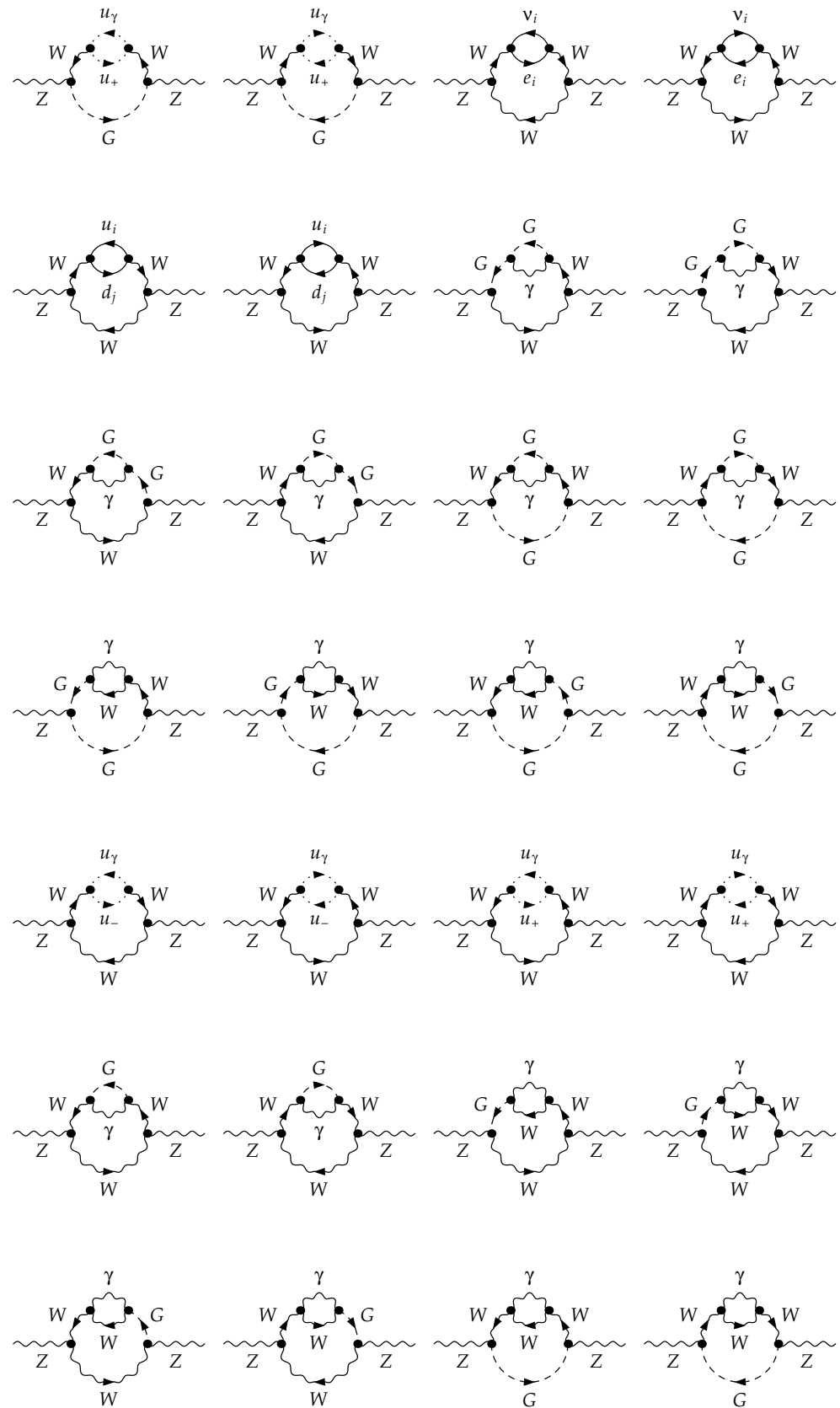


FIG. 12: Z self-energy diagrams which satisfy the 5th topology of Fig.3 and the cutting conditions of Fig.4.

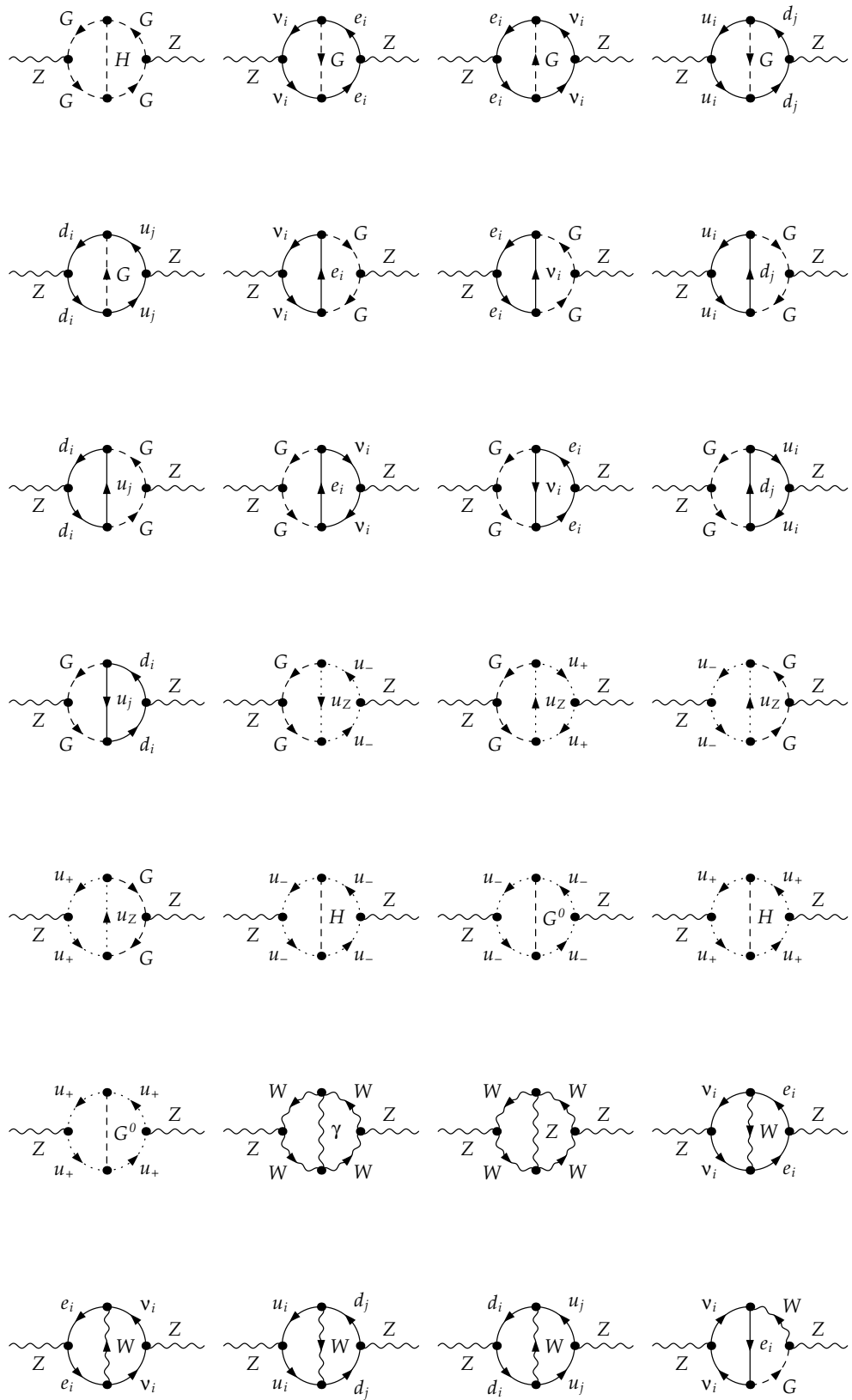
$$\begin{aligned}
& \times (4c_w^2 - 1 + c_w^2(8c_w^2 - 11)x_i) \theta[m_i - m_j - \sqrt{\xi_W}m_W] \\
& + \frac{\alpha^2 m_W^2}{192 c_w^4 s_w^4} (2c_W^2 + 1) \sum_{i=u,c} \sum_{j=d,s,b} \frac{1}{x_j} |V_{ij}|^2 C_{ij} \sqrt{1 - 4c_w^2 x_j} (\xi_W - x_j + x_i) \\
& \times (2c_w^2 + 1 + c_w^2(4c_w^2 - 7)x_j) \theta[m_j - m_i - \sqrt{\xi_W}m_W]. \tag{18}
\end{aligned}$$

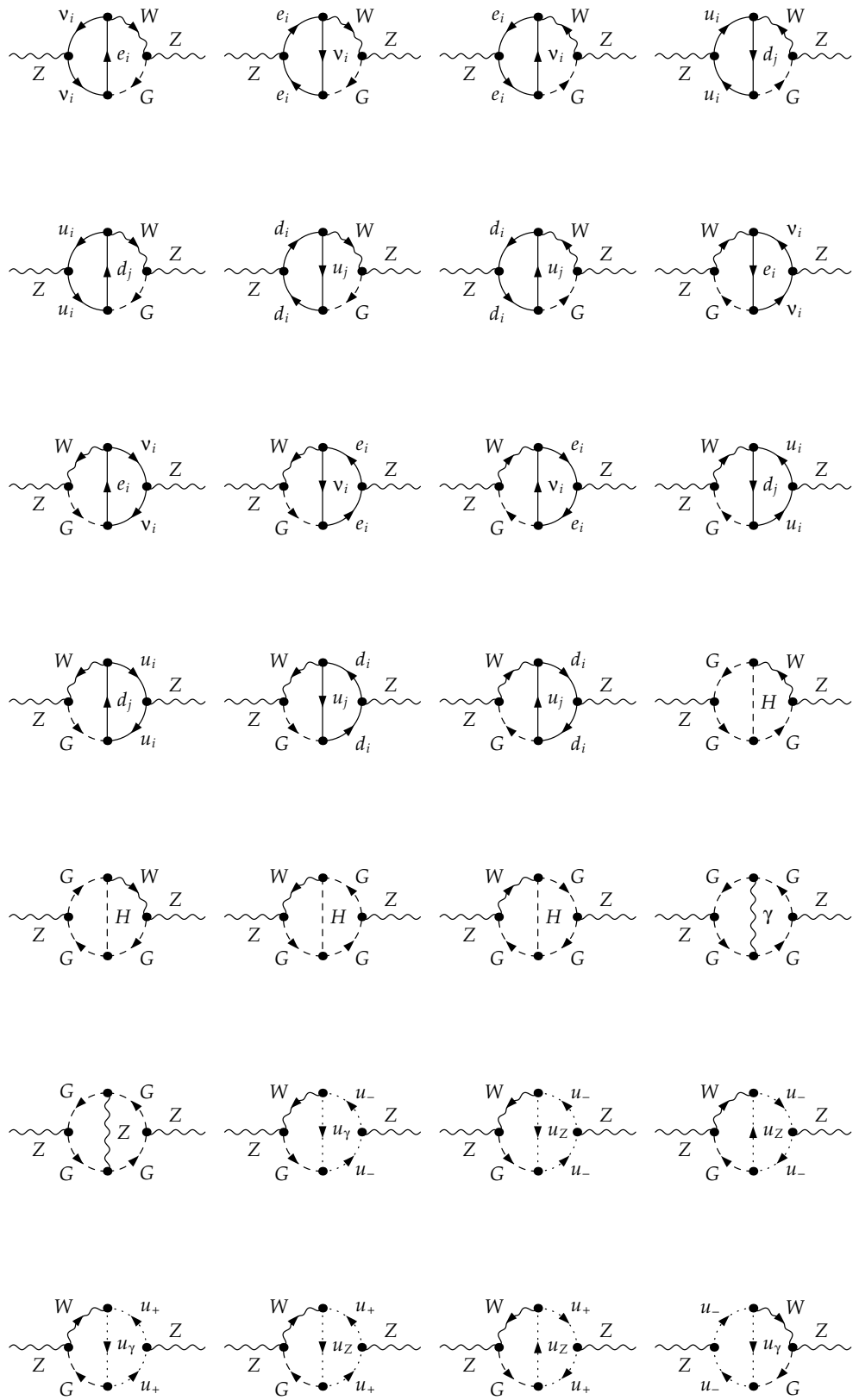
For the 6th topology of Fig.3 there are 124 Z self-energy diagrams as shown in Fig.13 which are ξ_W dependent and satisfy the cutting conditions of Fig.5. We will calculate the contributions of the five cuts of Fig.5 one by one. Firstly we obtain the ξ_W -dependent contribution of the first cut of Fig.5 to the real part of Z transverse self energy:

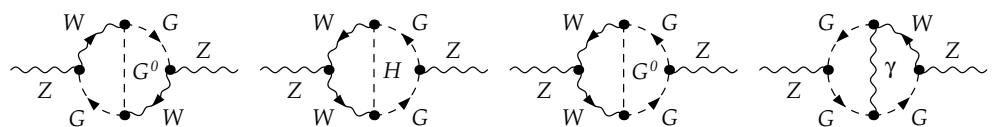
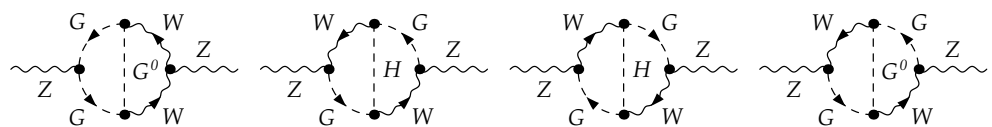
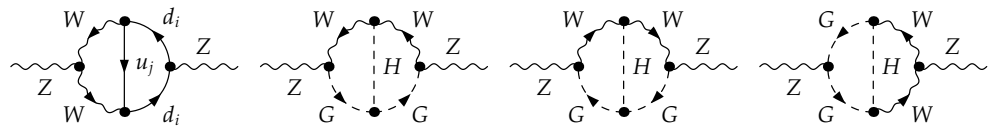
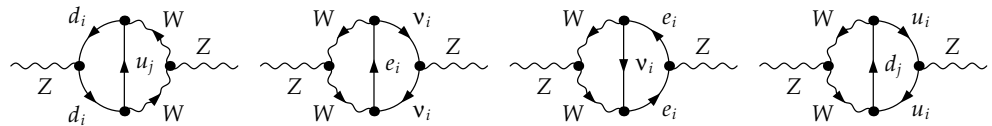
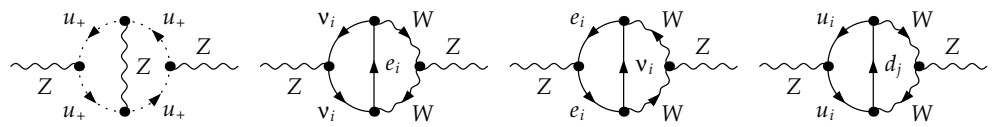
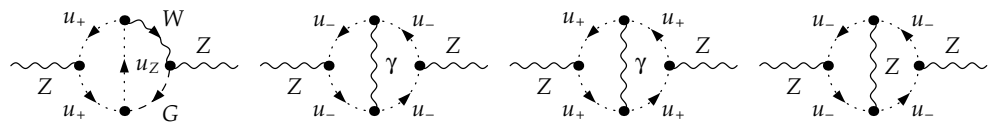
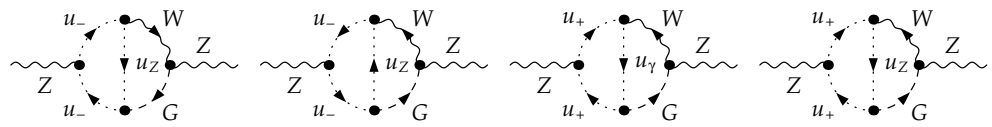
$$\begin{aligned}
Re\Sigma_{ZZ}^T(m_Z^2)|_{\xi_W-cut} &= \frac{\alpha^2 m_W^2}{4608 c_w^8 s_w^4} (1 - 4c_w^2 \xi_W)^3 (1 + 4c_w^4 - 2c_w^6) \theta\left[\frac{1}{c_w} - 2\sqrt{\xi_W}\right] \\
&- \frac{\alpha^2 m_W^2}{576 c_w^6 s_w^4} (1 - 4c_w^2 \xi_W)^{3/2} [3 + \left(\sum_{i=e,\mu,\tau} 2c_w^2 - 1 + c_w^2(4c_w^2 - 5)x_i\right. \\
&+ \left. \sum_{i=u,c} 4c_w^2 - 1 + c_w^2(8c_w^2 - 11)x_i + \sum_{i=d,s,b} 2c_w^2 + 1 + c_w^2(4c_W^2 - 7)x_i\right) \\
&\times \sqrt{1 - 4c_w^2 x_i}] \theta\left[\frac{1}{c_w} - 2\sqrt{\xi_W}\right] + \frac{\alpha^2 m_W^2}{1152 c_w^8 s_w^2} D \sqrt{1 - 4c_w^2 \xi_W} \\
&\times [4(\xi_W - 1)^2 \xi_W c_w^{10} + (4\xi_W^3 - 17\xi_W^2 + 46\xi_W - 1)c_w^8 \\
&+ (4\xi_W^3 + 55\xi_W^2 - 20\xi_W - 11)c_w^6 - (9\xi_W^2 + 42\xi_W - 6)c_w^4 \\
&+ (6\xi_W + 7)c_W^2 - 1] \theta\left[\frac{1}{c_W} - \sqrt{\xi_W} - 1\right] \\
&+ \frac{\alpha^2 m_W^2}{2304 c_w^8} [3(\xi_W - 1)^6 c_w^{14} + 2(\xi_W - 1)^4 (\xi_W^2 + 25\xi_W + 100)c_w^{12} \\
&- 3(\xi_W - 1)^2 (4\xi_W^3 + 85\xi_W^2 + 58\xi_W + 141)c_w^{10} \\
&+ 6(5\xi_W^4 + 74\xi_W^3 - 144\xi_W^2 - 50\xi_W - 13)c_w^8 \\
&- (40\xi_W^3 + 411\xi_W^2 - 798\xi_W - 581)c_w^6 + 6(5\xi_W^2 + 31\xi_W - 42)c_w^4 \\
&- 3(4\xi_W + 11)c_w^2 + 2] \theta\left[\frac{1}{c_w} - \sqrt{\xi_W} - 1\right] + \frac{\alpha^2 m_W^2}{288 c_w^6 s_w^2} D E \\
&\times [3 + \left(\sum_{i=e,\mu,\tau} (2c_w^2 - 1 + c_w^2(4c_w^2 - 5)x_i) + \sum_{i=u,c} (4c_w^2 - 1 + c_w^2(8c_w^2 - 11)x_i)\right. \\
&+ \left. \sum_{i=d,s,b} (2c_w^2 + 1 + c_w^2(4c_W^2 - 7)x_i)\right) \sqrt{1 - 4c_w^2 x_i}] \theta\left[\frac{1}{c_w} - \sqrt{\xi_W} - 1\right]. \tag{19}
\end{aligned}$$

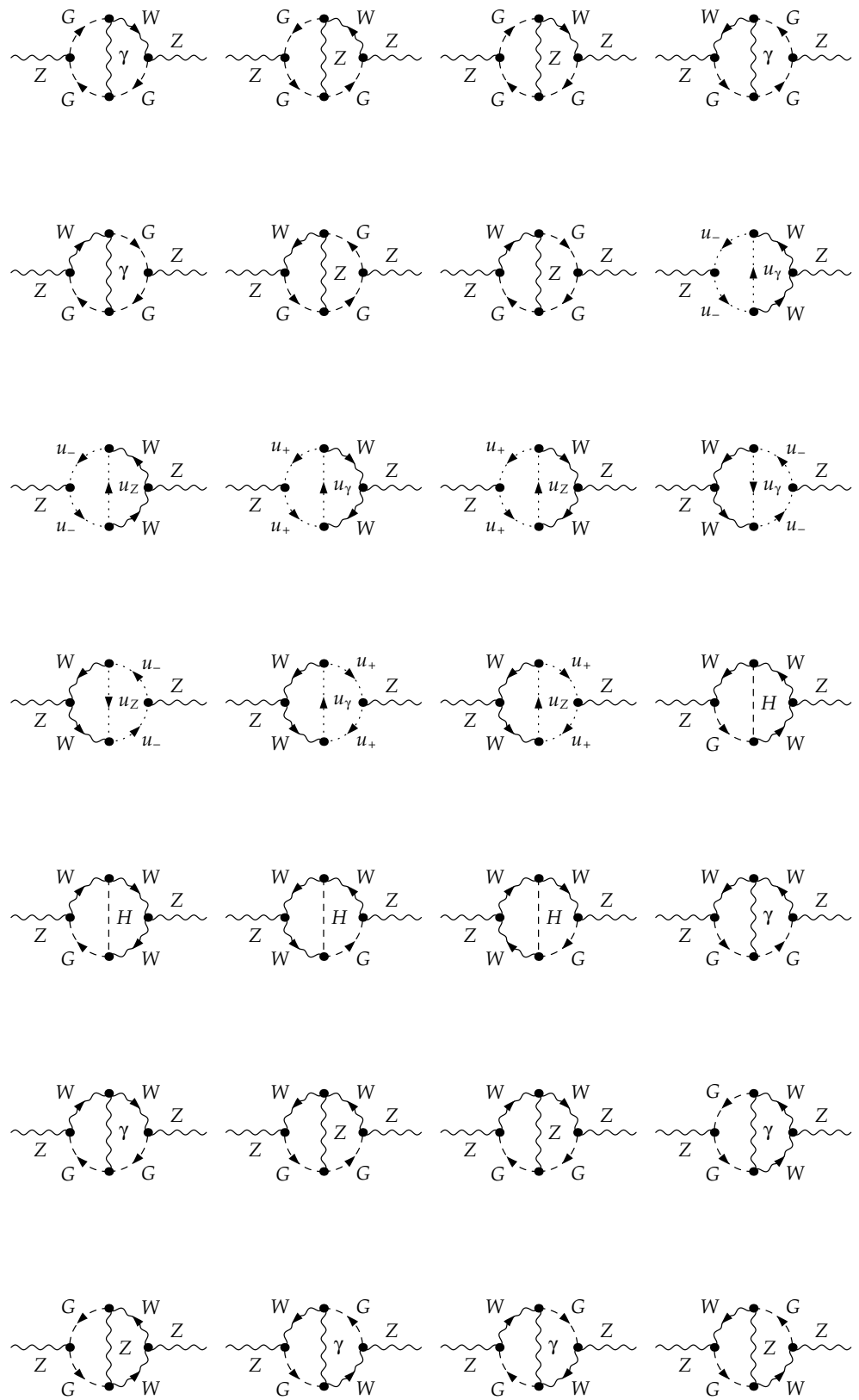
Then we obtain the ξ_W -dependent contribution of the second and third cuts of Fig.5 to the real part of Z transverse self energy:

$$\begin{aligned}
&Re\Sigma_{ZZ}^T(m_Z^2)|_{\xi_W-cut} \\
&= -\frac{\alpha^2 m_W^2}{384 c_w^2 s_w^2} D E \left[\sum_{i=e,\mu,\tau} (1 - x_i)^2 (2 + x_i) + 3 \sum_{i=u,c} \sum_{j=d,s,b} |V_{ij}|^2 A_{ij} B_{ij} \right] \theta\left[\frac{1}{c_w} - \sqrt{\xi_W} - 1\right]
\end{aligned}$$









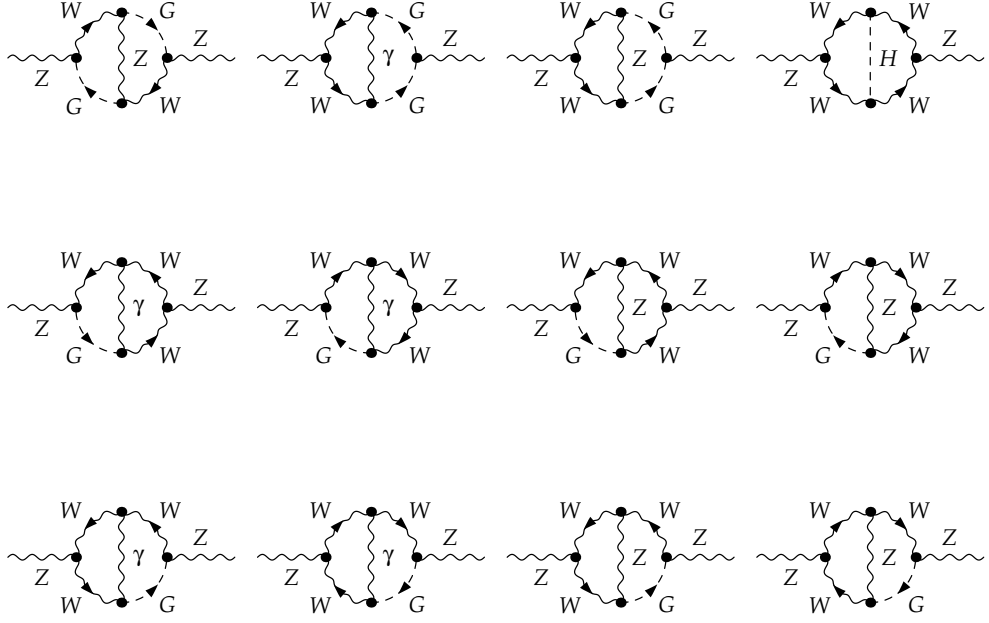


FIG. 13: ξ_W -dependent Z self-energy diagrams which satisfy the 6th topology of Fig.3 and the cutting conditions of Fig.5.

$$\begin{aligned}
& - \frac{\alpha^2 m_W^2}{1536 c_w^4} (\xi_W - 1) D [(\xi_W - 1)^3 (\xi_W^3 - \xi_W^2 - 3\xi_W - 33) c_w^6 \\
& - (\xi_W - 1)(3\xi_W^4 - 9\xi_W^3 - 29\xi_W^2 + 101\xi_W + 366) c_w^4 \\
& + (3\xi_W^4 - 10\xi_W^3 - 22\xi_W^2 + 170\xi_W - 93) c_w^2 - \xi_W^3 + 2\xi_W^2 + 5\xi_W - 18] \theta \left[\frac{1}{c_w} - \sqrt{\xi_W} - 1 \right] \\
& - \frac{\alpha^2 m_W^2}{128 s_w^4 \xi_W^2} (1 - 4 c_w^2 \xi_W)^{3/2} \sum_{i=e,\mu,\tau} x_i (x_i - \xi_W)^2 \theta \left[\frac{1}{c_w} - 2\sqrt{\xi_W} \right] \theta [\sqrt{\xi_W} m_W - m_i] \\
& - \frac{3 \alpha^2 m_W^2}{128 s_w^4 \xi_W^2} (1 - 4 c_w^2 \xi_W)^{3/2} \sum_{i=u,c} \sum_{j=d,s,b} |V_{ij}|^2 C_{ij} (\xi_W (x_i + x_j) - (x_i - x_j)^2) \\
& \times \theta \left[\frac{1}{c_w} - 2\sqrt{\xi_W} \right] \theta [\sqrt{\xi_W} m_W - m_i - m_j] + \frac{\alpha^2 m_W^2}{128 c_w^4 s_w^4} (2c_W^2 - 1) \\
& \times \sum_{i=e,\mu,\tau} \frac{1}{x_i} \sqrt{1 - 4 c_w^2 x_i} (x_i - \xi_W)^2 (2c_W^2 - 1 + c_w^2 (4c_W^2 - 5) x_i) \theta [m_i - \sqrt{\xi_W} m_W] \\
& - \frac{\alpha^2 m_W^2}{384 c_w^4 s_w^4} (4c_W^2 - 1) \sum_{i=u,c} \sum_{j=d,s,b} \frac{1}{x_i} |V_{ij}|^2 C_{ij} \sqrt{1 - 4 c_w^2 x_i} (\xi_W - x_i + x_j) \\
& \times (4c_W^2 - 1 + c_w^2 (8c_W^2 - 11) x_i) \theta [m_i - m_j - \sqrt{\xi_W} m_W] \\
& - \frac{\alpha^2 m_W^2}{384 c_w^4 s_w^4} (2c_W^2 + 1) \sum_{i=u,c} \sum_{j=d,s,b} \frac{1}{x_j} |V_{ij}|^2 C_{ij} \sqrt{1 - 4 c_w^2 x_j} (\xi_W - x_j + x_i) \\
& \times (2c_W^2 + 1 + c_w^2 (4c_W^2 - 7) x_j) \theta [m_j - m_i - \sqrt{\xi_W} m_W]. \tag{20}
\end{aligned}$$

From Fig.5 one readily sees the 4th and 5th cuts are right-and-left symmetric with the second and

third cuts. After careful calculations we also find the ξ_W -dependent contribution of the 4th and 5th cuts of Fig.5 to the real part of Z transverse self energy is equal to that of the second and third cuts of Fig.5.

Summing up all of the above results we obtain the gauge dependence of the part containing Heaviside functions of the real part of Z two-loop-level transverse self energy (see Eqs.(14-20) and the corresponding discussions)

$$\begin{aligned}
& Re \Sigma_{ZZ}^T(m_Z^2) |_{\xi_W-cut} \\
= & \frac{\alpha^2 m_W^2}{1728 c_w^6 s_w^2} \left[9 + 3 \sum_{i=e,\mu,\tau} \sqrt{1 - 4 c_w^2 x_i} (16 x_i c_w^6 + (8 - 24 x_i) c_w^4 + (7 x_i - 12) c_w^2 + 5) \right. \\
+ & \sum_{i=u,c} \sqrt{1 - 4 c_w^2 x_i} (64 x_i c_w^6 + (32 - 80 x_i) c_w^4 + (7 x_i - 40) c_w^2 + 17) \\
+ & \left. \sum_{i=d,s,b} \sqrt{1 - 4 c_w^2 x_i} (16 x_i c_w^6 + 8(1 - x_i) c_w^4 - (17 x_i + 4) c_w^2 + 5) \right] \\
\times & [2 D E \theta \left[\frac{1}{c_w} - \sqrt{\xi_W} - 1 \right] - \frac{1}{s_w^2} (1 - 4 c_w^2 \xi_W)^{3/2} \theta \left[\frac{1}{c_w} - 2 \sqrt{\xi_W} \right]].
\end{aligned} \tag{21}$$

This result proves that the part containing Heaviside functions of Z mass counterterm is gauge dependent under the on-shell mass renormalization prescription, i.e. the Z mass counterterm is gauge dependent under the on-shell mass renormalization prescription.

In order to calculate the gauge dependence of Z mass definition of the pole mass renormalization prescription we need to calculate the following term (see Eq.(5)):

$$\begin{aligned}
& m_Z \Gamma_Z \operatorname{Im} \Sigma_{ZZ}^{T'}(m_Z^2) |_{\xi_W-cut} \\
= & \frac{\alpha^2 m_W^2}{1728 c_w^6 s_w^2} \left[9 + 3 \sum_{i=e,\mu,\tau} \sqrt{1 - 4 c_w^2 x_i} (16 x_i c_w^6 + (8 - 24 x_i) c_w^4 + (7 x_i - 12) c_w^2 + 5) \right. \\
+ & \sum_{i=u,c} \sqrt{1 - 4 c_w^2 x_i} (64 x_i c_w^6 + (32 - 80 x_i) c_w^4 + (7 x_i - 40) c_w^2 + 17) \\
+ & \left. \sum_{i=d,s,b} \sqrt{1 - 4 c_w^2 x_i} (16 x_i c_w^6 + 8(1 - x_i) c_w^4 - (17 x_i + 4) c_w^2 + 5) \right] \\
\times & \left[\frac{1}{s_w^2} (1 - 4 c_w^2 \xi_W)^{3/2} \theta \left[\frac{1}{c_w} - 2 \sqrt{\xi_W} \right] - 2 D E \theta \left[\frac{1}{c_w} - \sqrt{\xi_W} - 1 \right] \right].
\end{aligned} \tag{22}$$

From Eq.(5) and Eqs.(21,22) we get the gauge dependence of the part containing Heaviside functions of Z mass counterterm under the pole mass renormalization prescription:

$$\delta m_Z^2 |_{\xi_W-cut} = 0 \quad \text{under pole mass renormalization prescription.} \tag{23}$$

C. Gauge dependence of the counterterm of the sine of the weak mixing angle under the two mass renormalization prescriptions

From the two-loop-level W and Z's mass counterterms we can calculate the two-loop-level counterterm of the sine of the weak mixing angle. To two-loop level one has [2]

$$\delta s_w = \frac{c_w^2}{2s_w} \left(\frac{\delta m_Z^2}{m_Z^2} - \frac{\delta m_W^2}{m_W^2} \right) + \frac{c_w^2}{2s_w} \left(\frac{\delta m_Z^2 \delta m_W^2}{m_Z^2 m_W^2} - \frac{(\delta m_Z^2)^2}{m_Z^4} \right) - \frac{c_w^4}{8s_w^3} \left(\frac{\delta m_Z^2}{m_Z^2} - \frac{\delta m_W^2}{m_W^2} \right)^2 + O(g^6). \quad (24)$$

The one-loop-level W and Z's mass counterterms have been proven gauge independent [6]. So we only need to calculate the gauge dependence of the first term of the r.h.s. of Eq.(24). From Eqs.(11,21) we obtain the gauge dependence of the part containing Heaviside functions of the two-loop-level δs_w under the on-shell mass renormalization prescription

$$\begin{aligned} \delta s_w|_{\xi_W-cut} = & \frac{\alpha^2}{3456 c_w^2 s_w^3} \left[9 + 3 \sum_{i=e,\mu,\tau} \sqrt{1 - 4 c_w^2 x_i} (16x_i c_w^6 + (8 - 24x_i)c_w^4 + (7x_i - 12)c_w^2 + 5) \right. \\ & + \sum_{i=u,c} \sqrt{1 - 4 c_w^2 x_i} (64x_i c_w^6 + (32 - 80x_i)c_w^4 + (7x_i - 40)c_w^2 + 17) \\ & + \sum_{i=d,s,b} \sqrt{1 - 4 c_w^2 x_i} (16x_i c_w^6 + 8(1 - x_i)c_w^4 - (17x_i + 4)c_w^2 + 5) \left. \right] \\ & \times [2D E \theta \left[\frac{1}{c_w} - \sqrt{\xi_W} - 1 \right] - \frac{1}{s_w^2} (1 - 4 c_w^2 \xi_W)^{3/2} \theta \left[\frac{1}{c_w} - 2\sqrt{\xi_W} \right]] \\ & + \frac{\alpha^2 c_w^2}{1152 s_w^3} \left[3 \sum_{i=u,c} \sum_{j=d,s,b} |V_{ij}|^2 A_{ij} B_{ij} + \sum_{i=e,\mu,\tau} (1 - x_i)^2 (2 + x_i) \right] \\ & \times (1 - \xi_W)(\xi_W^2 - 2\xi_W - 11) \theta[1 - \xi_W] \quad \text{under on-shell prescription.} \quad (25) \end{aligned}$$

Eq.(25) implies δs_w is gauge dependent under the on-shell mass renormalization prescription. On the other hand, from Eqs.(13,23) we obtain the gauge dependence of the part containing Heaviside functions of the two-loop-level δs_w under the pole mass renormalization prescription

$$\delta s_w|_{\xi_W-cut} = 0 \quad \text{under pole prescription.} \quad (26)$$

III. GAUGE DEPENDENCE OF PHYSICAL RESULT UNDER THE ON-SHELL AND POLE MASS RENORMALIZATION PRESCRIPTIONS

From the results of section II we have found the counterterms of W and Z's mass and the sine of the weak mixing angle are gauge dependent under the on-shell mass renormalization prescription, but those gauge dependencies don't appear in the counterterms of the pole mass renormalization prescription. Maybe this conclusion is not enough to judge which renormalization prescription is

reasonable. So we will judge the reasonableness of the two renormalization prescriptions from the gauge independence of physical result.

For example we calculate the gauge dependence of the two-loop-level cross section of the physical process $\mu \rightarrow \nu_\mu e^- \bar{\nu}_e$ under the two mass renormalization prescriptions. Note that we only calculate the gauge dependence of the part containing the Heaviside functions $\theta[1 - \xi_W]$, $\theta[1/c_w - \sqrt{\xi_W} - 1]$ and $\theta[1/c_w - 2\sqrt{\xi_W}]$ of the cross section of the physical process. This will not affect our conclusion. Under this consideration only the diagrams containing the two-loop-level counterterms δs_w and δm_W^2 as shown in Fig.14 need to be calculated. This is because: 1) all of the one-loop-level physical

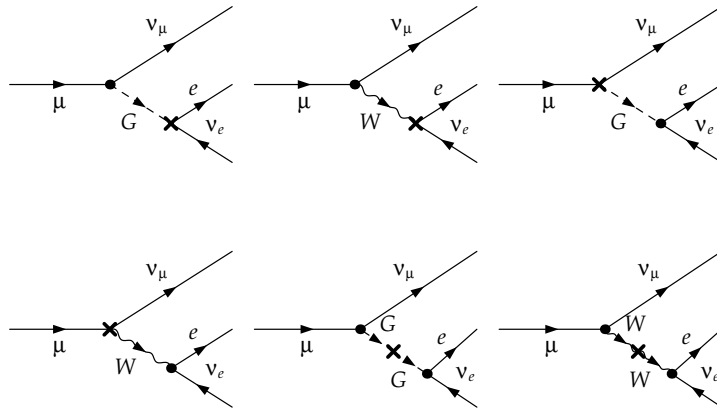


FIG. 14: Diagrams of $\mu \rightarrow \nu_\mu e^- \bar{\nu}_e$ containing the two-loop-level counterterms δs_w and δm_W^2 .

parameter's counterterms and the two-loop-level counterterms of the lepton masses and electron charge don't contain the Heaviside functions $\theta[1 - \xi_W]$, $\theta[1/c_w - \sqrt{\xi_W} - 1]$ and $\theta[1/c_w - 2\sqrt{\xi_W}]$; 2) the energy of the incoming particle of this process is order of muon energy which doesn't reach the threshold of the singularities containing the Heaviside functions $\theta[1 - \xi_W]$, $\theta[1/c_w - \sqrt{\xi_W} - 1]$ and $\theta[1/c_w - 2\sqrt{\xi_W}]$, thus all of loop momentum integrals of the Feynman diagrams don't contribute to these Heaviside functions. We can easily get the contribution of Fig.14 to the physical amplitude $\mu \rightarrow \nu_\mu e^- \bar{\nu}_e$

$$\begin{aligned} \mathcal{M}(\mu \rightarrow \nu_\mu e^- \bar{\nu}_e) \rightarrow & \frac{4\pi\alpha(m_e m_\mu F_1 - m_W^2 F_2)}{m_W^2 s_w^3 (m_W^2 - m_e^2 - 2q_2 \cdot q_3)} \delta s_w + \frac{2\pi\alpha \delta m_W^2}{m_W^4 s_w^2 (m_W^2 - m_e^2 - 2q_2 \cdot q_3)^2} \\ & \times [m_e m_\mu (2m_W^2 - m_e^2 - 2q_2 \cdot q_3) F_1 - m_W^4 F_2], \end{aligned} \quad (27)$$

where m_e and m_μ is the mass of electron and muon, q_2 and q_3 are the momentums of electron and the anti electron neutrino, and

$$F_1 = \bar{u}(q_1) \gamma_R u(p) \bar{u}(q_2) \gamma_L \nu(q_3), \quad F_2 = \bar{u}(q_1) \gamma^\mu \gamma_L u(p) \bar{u}(q_2) \gamma_\mu \gamma_L \nu(q_3), \quad (28)$$

where p and q_1 are the momentums of muon and muon neutrino, and γ_L and γ_R are the left- and right- handed helicity operators. The contribution of Eq.(27) to the two-loop-level cross section of $\mu \rightarrow \nu_\mu e^- \bar{\nu}_e$ is

$$\begin{aligned} \sigma(\mu \rightarrow \nu_\mu e^- \bar{\nu}_e) &\propto |\mathcal{M}(\mu \rightarrow \nu_\mu e^- \bar{\nu}_e)|^2 \\ &\rightarrow \frac{16\pi^2\alpha^2 q_1 \cdot q_2 (m_e^2 - m_\mu^2 + 2q_1 \cdot q_2)}{m_W^4 s_w^4} \left(\frac{2\delta s_w}{s_w} + \frac{\delta m_W^2}{m_W^2} \right). \end{aligned} \quad (29)$$

In Eq.(29) we have averaged the result over the incoming fermion's helicity states and summed up the results for the different outgoing fermions' helicity states. On the other hand we only keep the lowest order of the quantities m_e^2/m_W^2 , m_μ^2/m_W^2 and so on in Eq.(29), since the energies of the external-line particles are very small compared with m_W^2 .

From Eqs.(11,25) and Eq.(29) we obtain the gauge dependence of the part containing the Heaviside functions $\theta[1 - \xi_W]$, $\theta[1/c_w - \sqrt{\xi_W} - 1]$ and $\theta[1/c_w - 2\sqrt{\xi_W}]$ of the two-loop-level cross section of $\mu \rightarrow \nu_\mu e^- \bar{\nu}_e$ under the on-shell mass renormalization prescription

$$\begin{aligned} \sigma_2(\mu \rightarrow \nu_\mu e^- \bar{\nu}_e)_{\xi_W-cut} &\rightarrow \frac{\pi^2\alpha^4 q_1 \cdot q_2 (m_e^2 - m_\mu^2 + 2q_1 \cdot q_2)}{108m_W^4 c_w^2 s_w^8} \left[9 \right. \\ &+ 3 \sum_{i=e,\mu,\tau} \sqrt{1 - 4c_w^2 x_i} (16x_i c_w^6 + (8 - 24x_i)c_w^4 + (7x_i - 12)c_w^2 + 5) \\ &+ \sum_{i=u,c} \sqrt{1 - 4c_w^2 x_i} (64x_i c_w^6 + (32 - 80x_i)c_w^4 + (7x_i - 40)c_w^2 + 17) \\ &+ \sum_{i=d,s,b} \sqrt{1 - 4c_w^2 x_i} (16x_i c_w^6 + 8(1 - x_i)c_w^4 - (17x_i + 4)c_w^2 + 5) \left. \right] \\ &\times [2D E \theta\left[\frac{1}{c_w} - \sqrt{\xi_W} - 1\right] - \frac{1}{s_w^2} (1 - 4c_w^2 \xi_W)^{3/2} \theta\left[\frac{1}{c_w} - 2\sqrt{\xi_W}\right]] \\ &+ \frac{\pi^2\alpha^4 q_1 \cdot q_2 (m_e^2 - m_\mu^2 + 2q_1 \cdot q_2)}{36m_W^4 s_w^8} (2c_w^2 - 1)(1 - \xi_W)(\xi_W^2 - 2\xi_W - 11) \\ &\times \left[3 \sum_{i=u,c} \sum_{j=d,s,b} |V_{ij}|^2 A_{ij} B_{ij} + \sum_{i=e,\mu,\tau} (1 - x_i)^2 (2 + x_i) \right] \theta[1 - \xi_W]. \end{aligned} \quad (30)$$

Eq.(30) implies the on-shell mass renormalization prescription makes the cross section of the physical process $\mu \rightarrow \nu_\mu e^- \bar{\nu}_e$ gauge dependent. So the on-shell mass renormalization prescription is a wrong mass renormalization prescription beyond one-loop level. The quantitative order of this gauge dependence can be seen in Fig.15. In Fig.15 the following data have been used: $e = 0.3028$, $s_w^2 = 0.2312$, $m_W = 80.42\text{Gev}$, $m_u = 3\text{Mev}$, $m_c = 1.25\text{Gev}$, $m_t = 174.3\text{Gev}$, $m_d = 6\text{Mev}$, $m_s = 120\text{Mev}$, $m_b = 4.2\text{Gev}$, $m_e = 0.5110\text{Mev}$, $m_\mu = 105.7\text{Mev}$, $m_\tau = 1.777\text{Gev}$, $|V_{ud}| = 0.975$, $|V_{us}| = 0.223$, $|V_{ub}| = 0.004$, $|V_{cd}| = 0.222$, $|V_{cs}| = 0.974$, $|V_{cb}| = 0.040$, $|V_{td}| = 0.009$, $|V_{ts}| = 0.039$, and $|V_{tb}| = 0.999$ [13]. Obviously the gauge dependence of $\sigma(\mu \rightarrow \nu_\mu e^- \bar{\nu}_e)$ induced by the on-shell mass renormalization prescription cannot be neglected at the two-loop level. On the other hand,

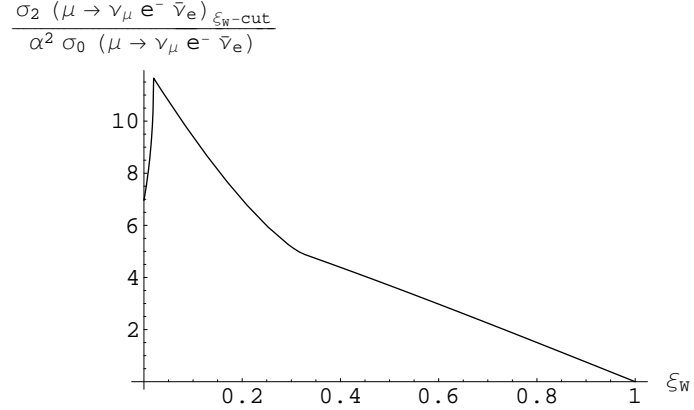


FIG. 15: Gauge dependence of the two-loop-level cross section of $\mu \rightarrow \nu_\mu e^- \bar{\nu}_e$ under the on-shell mass renormalization prescription, where $q_1 \cdot q_2 = q_2 \cdot q_3 = m_\mu^2/6 - m_e^2/2$ and $\sigma_0(\mu \rightarrow \nu_\mu e^- \bar{\nu}_e)$ is the tree-level cross section.

from Eqs.(13,26) and Eq.(29) we find such gauge dependence doesn't appear in the result of the pole mass renormalization prescription.

IV. CONCLUSION

Through calculating the singularities of W and Z's two-loop-level transverse self energy we find the counterterms of W and Z's mass and the sine of the weak mixing angle are gauge dependent under the on-shell mass renormalization prescription. The gauge dependencies of these counterterms lead to the cross section of $\mu \rightarrow \nu_\mu e^- \bar{\nu}_e$ gauge dependent at two-loop level. So the on-shell mass renormalization prescription is a wrong mass renormalization prescription beyond one-loop level.

On the other hand, all of the above gauge dependencies don't appear in the results of the pole mass renormalization prescription. So the pole mass renormalization prescription is the only reasonable candidate for the mass renormalization prescription at present. We should use the pole mass renormalization prescription rather than the on-shell mass renormalization prescription to calculate physical results beyond one-loop level.

Acknowledgments

The author thanks Prof. Xiao-Yuan Li and Prof. Cai-dian Lu for their useful guidance.

- [1] M. Veltman, *Physica* **29** (1963) 186;
- D. Bardin and G. Passarino, *The Standard Model in the Making Precision Study of the Electroweak Interactions*, Oxford Science Pub., Clarendon Press, Oxford,1999.
- [2] A. Denner, *Fortschr. Phys.* **41** (1993) 307.
- [3] A.Sirlin, *Phys. Rev. Lett.* **67** (1991) 2127; *Phys. Lett. B* **267** (1991) 240;
 R.G. Stuart, *Phys. Lett. B* **272** (1991) 353.
- [4] M. Passera, A. Sirlin, *Phys. Rev. Lett.* **77** (1996) 4146;
 B.A. Kniehl, A. Sirlin, *Phys. Rev. Lett.* **81** (1998) 1373;
 P.A. Grassi, B.A. Kniehl and A. Sirlin, *Phys. Rev. Lett.* **86** (2001) 389;
 M.L. Nekrasov, *Phys. Lett. B* **531** (2002) 225;
 B.A. Kniehl, A. Sirlin, *Phys. Lett. B* **530** (2002) 129;
- [5] J.C. Breckenridge, M.J. Lavelle, T.G. Steele, *Z. Phys. C* **65** (1995) 155.
- [6] P. Gambino, P.A. Grassi, *Phys. Rev. D* **62** (2000) 076002 (hep-ph/9907254).
- [7] N.K. Nielsen, *Nucl. Phys. B* **101** (1975) 173;
 R. Tarrach, *Nucl. Phys. B* **183** (1981) 384;
 O. Piguet and K. Sibold, *Nucl. Phys. B* **253** (1985) 517;
 N. Gray, D.J. Broadhurst, W. Grafe, K. Schilcher, *Z. Phys. C* **48** (1990) 673;
 D.J. Broadhurst, N. Gray, K. Schilcher, *Z. Phys. C* **52** (1991) 111.
- [8] J. Kublbeck, M. Bohm, A. Denner, *Comput. Phys. Commun.* **60** (1990) 165;
 G.J. van Oldenborgh, J.A.M. Vermaasen, *Z. Phys. C* **46** (1990) 425;
 T. Hahn, M. Perez-Victoria, *Comput. Phys. Commun.* **118** (1999) 153.
- [9] J. Gegelia, G. Japaridze, A. Tkabladze, A. Khelashvili, K. Turashvili, hep-ph/9910527;
 F. Jegerlehner, M.Yu. Kalmykov and O. Veretin, *Nucl. Phys. B* **641** (2002) 285;
 F. Jegerlehner, M.Yu. Kalmykov and O. Veretin, *Nucl. Phys. B* **658** (2003) 49.
- [10] A. Freitas, W. Hollik, W. Walter, G. Weiglein, *Phys. Lett. B* **495** (2000) 338;
 A. Freitas, W. Hollik, W. Walter, G. Weiglein, *Nucl. Phys. B* **632** (2002) 189.
- [11] N.Cabibbo, *Phys. Rev. Lett.* **10**, 531 (1963);
 M.Kobayashi and K.Maskawa, *Prog. Theor. Phys.* **49** (1973) 652.
- [12] R.E. Cutkosky, *J. Math. Phys.* **1**, 429 (1960);
 Yong Zhou, hep-ph/0508225.
- [13] The European Physical Journal C, 15 (2000) 1-878.

Gauge dependence of on-shell and pole mass renormalization prescriptions

Yong Zhou

*Beijing University of Posts and Telecommunications,
school of science P.O. Box 123, Beijing 100876, China*

We discuss the gauge dependence of physical parameter's definitions under the on-shell and pole mass renormalization prescriptions. By two-loop-level calculations we prove for the first time that the on-shell mass renormalization prescription makes physical result gauge dependent. On the other hand, such gauge dependence doesn't appear in the result of the pole mass renormalization prescription. Our calculation also implies the difference of the physical results between the two mass renormalization prescriptions cannot be neglected at two-loop level.

PACS numbers: 11.10.Gh, 12.15.Lk

I. INTRODUCTION

The conventional on-shell mass renormalization prescription has been present for a long time. It renormalizes the real part of particle's inverse propagator to zero at physical mass point. For boson the on-shell mass renormalization condition is [1, 2]

$$m^2 - m_0^2 + \text{Re}\Sigma(m^2) = 0, \quad (1)$$

where m_0 is the bare mass and Σ is the boson's diagonal self energy (for vector boson it is the transverse diagonal self energy). But recently people proposed a new mass renormalization prescription which renormalizes both the real and the imaginary parts of the particle's inverse propagator to zero at the (complex) pole of the particle's propagator, i.e. [3, 4]

$$\bar{s} - m_0^2 + \Sigma(\bar{s}) = 0, \quad (2)$$

where \bar{s} is the pole of the particle's propagator. Written $\bar{s} = m_2^2 - im_2\Gamma_2$, m_2 is defined as the physical mass of the particle [3]. Putting the expression of \bar{s} into Eq.(2) one has [3, 4]

$$m_2^2 - m_0^2 + \text{Re}\Sigma(\bar{s}) = 0, \quad m_2\Gamma_2 = \text{Im}\Sigma(\bar{s}). \quad (3)$$

By expanding Eqs.(3) at $\bar{s} = m_2^2$ one readily has (see Eq.(1)) [3, 4]

$$m - m_2 = \Gamma_2 \text{Im}\Sigma'(m_2^2)/2 + O(g^6), \quad (4)$$

where $\Sigma'(m_2^2) = \partial\Sigma(m_2^2)/\partial p^2$ and g is a generic coupling constant. For unstable boson the r.h.s. of Eq.(4) is gauge dependent [3, 4]. So A. Sirlin et al. claim that the on-shell mass definition m of unstable particles is gauge dependent, since the pole mass definition m_2 is gauge independent [3, 4, 5, 6].

But the conclusion that the pole mass definition m_2 is gauge independent has been proposed for not very long time. We still need to search new and stricter proofs to prove this conclusion. In this paper we will discuss if the pole mass definition is gauge independent and investigate the difference of physical result between the on-shell and pole mass renormalization prescriptions. The arrangement of this paper is as follows: firstly we discuss the gauge dependencies of the counterterms of gauge boson W and Z's mass and the sine of the weak mixing angle under the on-shell and pole mass renormalization prescriptions; then we discuss the gauge dependence of the two-loop-level cross section of the physical process $\mu \rightarrow \nu_\mu e^- \bar{\nu}_e$ under the two mass renormalization prescriptions; Lastly we give the conclusion.

II. GAUGE DEPENDENCIES OF PHYSICAL PARAMETER'S COUNTERTERMS UNDER THE ON-SHELL AND POLE MASS RENORMALIZATION PRESCRIPTIONS

The gauge invariance of Lagrangian always requires the bare physical parameters are gauge independent. The natural deduction of this conclusion is the counterterms of physical parameters should also be gauge independent [7], since the bare physical parameter can be divided into physical parameter and the corresponding counterterm, and the physical parameter is of course gauge independent. This criterion could be used to judge which mass renormalization prescription is reasonable, in other words which mass definition is gauge independent. In the following we will discuss the gauge dependence of the counterterms of gauge boson W and Z's mass and the sine of the weak mixing angle under the on-shell and pole mass renormalization prescriptions. For convenience we only discuss the dependence of W gauge parameter ξ_W in the R_ξ gauge, and we only introduce physical parameter's counterterms (i.e. we don't introduce field renormalization constants). The computer program packages *FeynArts* and *FeynCalc* [8] have been used in the following calculations. Here we note there are some early two-loop-level calculations about the massive gauge boson's self energies in Ref.[9].

From Eqs.(1,3) one has for massive gauge boson [10]

$$\begin{aligned}\delta m^2 &= Re\Sigma^T(m^2), \\ \delta m_2^2 &= Re\Sigma^T(m_2^2) + m_2\Gamma_2 Im\Sigma^{T'}(m_2^2) + O(g^6),\end{aligned}\quad (5)$$

where Σ^T denotes the transverse self energy of the gauge boson. The one-loop-level mass counterterms of W and Z have been proven gauge independent [6]. So we only need to discuss the two-loop-level case. Firstly m and m_2 should be regarded as equal quantities, since both of them are regarded as the physical mass of the same particle. Therefore we find the two-loop-level difference of the two mass counterterm is $m\Gamma Im\Sigma^{T'}(m^2)$. Every part of this term contains gauge-parameter-dependent Heaviside functions (which come from the one-loop-level $Im\Sigma^{T'}$ [3, 4]). So in order to discuss the difference of the gauge dependence of the two mass counterterms we only need to calculate the gauge dependence of the singularities of the two-loop-level $Re\Sigma^T(m^2)$, because only the singularities of $Re\Sigma^T(m^2)$ in $Re\Sigma^T(m^2)$ contain Heaviside functions. In other words for our purpose we only need to discuss the gauge dependence of the part which contains Heaviside functions of the two mass counterterms.

The two-loop-level self energies of gauge bosons can be classified into two kinds: one kind contains one-loop-level counterterms, the other kind doesn't contain any counterterm. Since except for CKM matrix elements [11] all of the one-loop-level counterterms of physical parameters are real numbers and don't contain Heaviside function [2], the first kind self energy doesn't contribute to the singularities of the real part of the gauge boson's self energy, because except the one-loop-level counterterm the left part of this kind self energy is an one-loop-level self energy which real part doesn't contain singularities. Here we don't need to worry about the problem that the CKM matrix elements and their counterterms are complex numbers, because the total contribution of them to the real part of the gauge boson's self energy is real number (the correctness of this conclusion can be seen in the following calculations). So we only need to calculate the contributions of the second kind self energy.

According to the *cutting rules* [12] the second kind self energy of gauge bosons can be classified into three kinds: one kind doesn't contain singularity, the second kind contains singularities, but its singularities don't contribute to the real part of the gauge boson's self energy, the third kind contains singularities and its singularities contribute to the real part of the gauge boson's self energy. The topologies of the three kind self energies are shown in Fig.1, Fig.2 and Fig.3. Here we note the middle propagator (denoted by broken line) in the one-particle-reducible diagrams of Fig.(1-3) is different from the external-line particles. The tadpole diagrams are also included in Fig.(1-3), because we don't introduce the tadpole counterterm [6].

Obviously we only need to calculate the contribution of the singularities of Fig.3 to the real part of the gauge boson's self energy. In Fig.3 we also draw the possible cuts/singularities of the first four topologies which contribute to the real part of the gauge boson's self energy (the arrow

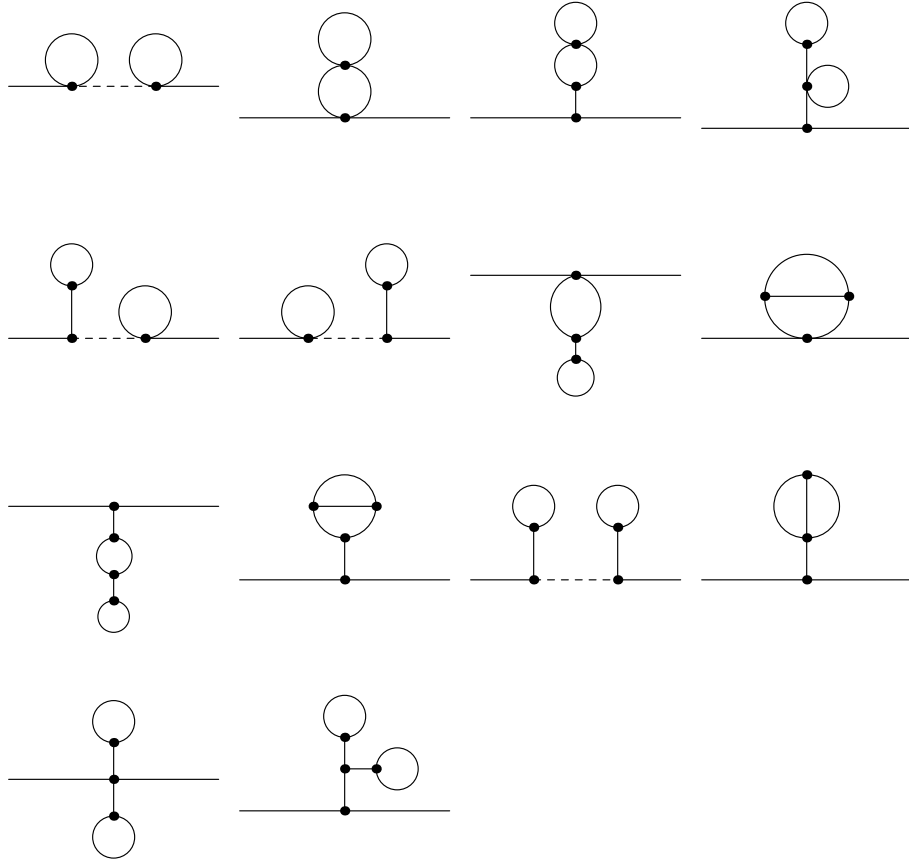


FIG. 1: Topologies of the two-loop-level self energy which lacks counterterm and singularity.

on the inner line denotes the corresponding propagator is cut [12]). The possible cuts of the left two topologies which contribute to the real part of the gauge boson's self energy are shown in Fig.4 and Fig.5.

A. Gauge dependence of W mass counterterm under the two mass renormalization prescriptions

In the standard model of particle physics the first topology of Fig.3 doesn't contribute to W transverse self energy, so we don't need to calculate its contribution. For the second topology of Fig.3 there are 39 Feynman diagrams in the standard model, but none of them satisfies the corresponding cutting condition. The case of the third topology of Fig.3 is same as the case of the second topology. For the 4th topology of Fig.3 there are two W self energy diagrams as shown in Fig.6 which satisfy the corresponding cutting condition. Using the cutting rules we obtain the gauge-parameter-dependent contribution of the cuts of Fig.6 to the real part of W transverse self

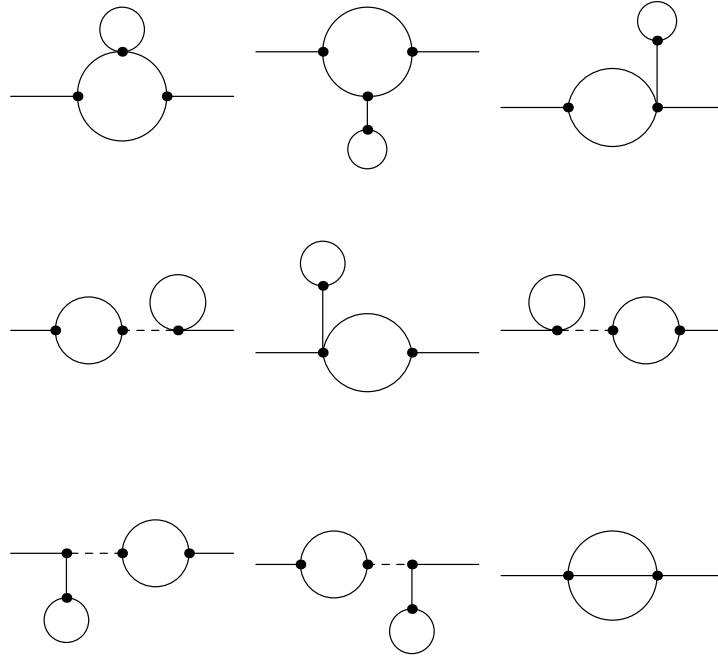


FIG. 2: Topologies of the two-loop-level self energy which lacks counterterm and its singularities don't contribute to the real part of the self energy.

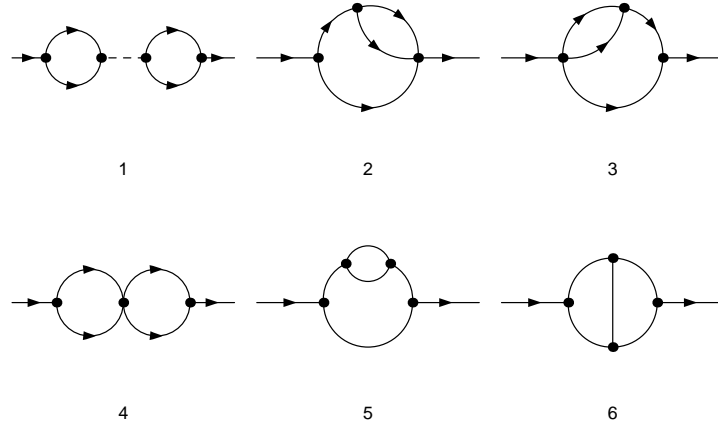


FIG. 3: Topologies of the two-loop-level self energy which lacks counterterm and its singularities contribute to the real part of the self energy.

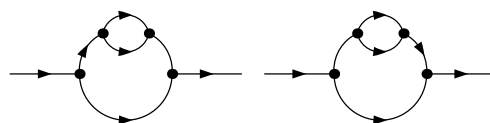


FIG. 4: Possible cuts of the 5th topology of Fig.3 which contribute to the real part of the self energy.

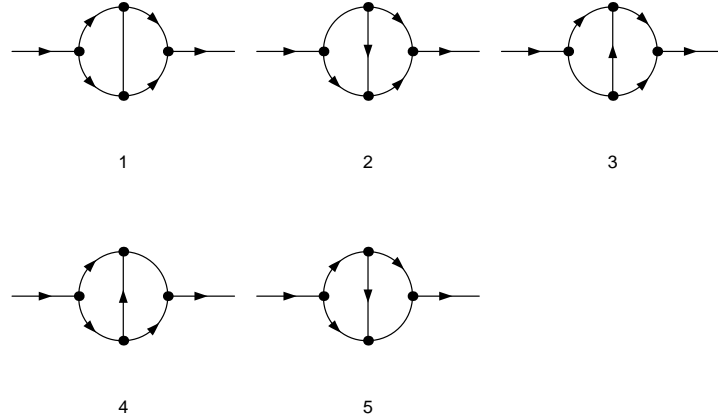


FIG. 5: Possible cuts of the 6th topology of Fig.3 which contribute to the real part of the self energy.

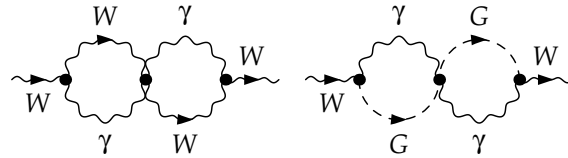


FIG. 6: W self energy diagrams which satisfy the 4th topology of Fig.3 and the corresponding cutting condition.

energy:

$$Re\Sigma_{WW}^T(m_W^2)|_{\xi_W-cut} = \frac{\alpha^2 m_W^2}{4608} (1 - \xi_W)^3 (\xi_W^5 - 3\xi_W^4 - 6\xi_W^3 - 46\xi_W^2 + 165\xi_W + 465) \theta[1 - \xi_W], \quad (6)$$

where Σ_{WW}^T is W transverse self energy, m_W and ξ_W is W's mass and gauge parameter, α is the fine structure constant, θ is the Heaviside function, and the subscript ξ_W-cut denotes the ξ_W -dependent contribution from the cuts/singularities. In the follows we restrict ourselves to $\xi_W > 0$ [4].

For the 5th topology of Fig.3 there are 14 W's self energy diagrams as shown in Fig.7 which are ξ_W -dependent and satisfy the cutting conditions of Fig.4. After careful calculations we obtain the gauge-parameter-dependent contribution of the cuts of Fig.7 to the real part of W transverse self energy:

$$\begin{aligned} Re\Sigma_{WW}^T(m_W^2)|_{\xi_W-cut} = & \frac{\alpha^2 m_W^2}{128s_w^4} \left[\sum_{i=e,\mu,\tau} \frac{1}{x_i} (1 - x_i)(x_i - \xi_W)^2 (x_i^2 + x_i - 2) \theta[m_i - \sqrt{\xi_W} m_W] \right. \\ & + \frac{1}{\xi_W^2} s_w^2 (1 - \xi_W)^3 \sum_{i=e,\mu,\tau} x_i (x_i - \xi_W)^2 \theta[\sqrt{\xi_W} m_W - m_i] \theta[1 - \xi_W] \\ & \left. + 3 \sum_{i=u,c} \sum_{j=d,s,b} \frac{1}{x_i} |V_{ij}|^2 (\xi_W - x_i + x_j) A_{ij} B_{ij} C_{ij} \theta[m_i - m_j - \sqrt{\xi_W} m_W] \right] \end{aligned}$$

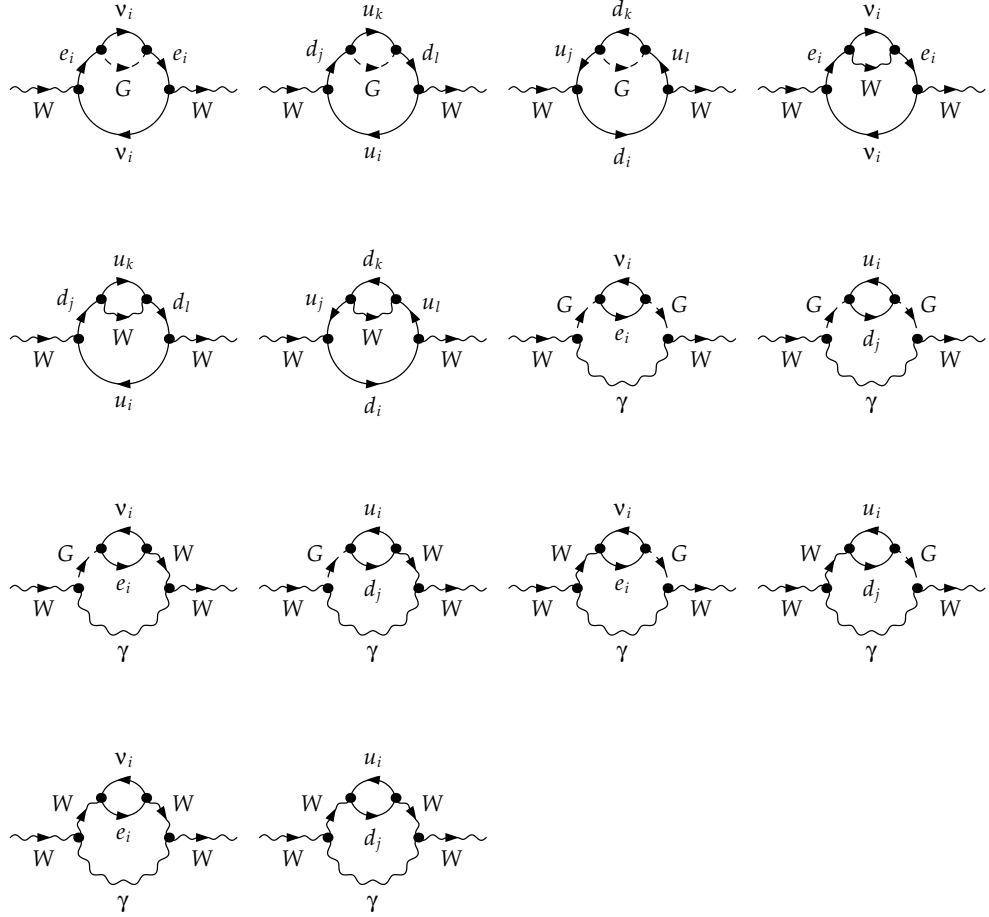


FIG. 7: ξ_W -dependent W self energy diagrams which satisfy the 5th topology of Fig.3 and the cutting conditions of Fig.4.

$$\begin{aligned}
& + 3 \sum_{i=u,c} \sum_{j=d,s,b} \frac{1}{x_j} |V_{ij}|^2 (\xi_W - x_j + x_i) A_{ij} B_{ij} C_{ij} \theta[m_j - m_i - \sqrt{\xi_W} m_W] \\
& + \frac{3}{\xi_W^2} s_w^2 (1 - \xi_W)^3 \sum_{i=u,c} \sum_{j=d,s,b} |V_{ij}|^2 (\xi_W (x_i + x_j) - (x_i - x_j)^2) C_{ij} \\
& \times \theta[\sqrt{\xi_W} m_W - m_i - m_j] \theta[1 - \xi_W] \Big] , \tag{7}
\end{aligned}$$

where s_w is the sine of the weak mixing angle, $x_i = m_i^2/m_W^2$, $x_j = m_j^2/m_W^2$, V_{ij} is the CKM matrix element [11], and

$$\begin{aligned}
A_{ij} &= \sqrt{(x_i - x_j)^2 - 2(x_i + x_j) + 1} , \\
B_{ij} &= 2 - (x_i + x_j) - (x_i - x_j)^2 , \\
C_{ij} &= \sqrt{(x_i - x_j)^2 - 2\xi_W(x_i + x_j) + \xi_W^2} . \tag{8}
\end{aligned}$$

For the 6th topology of Fig.3 there are 53 W self energy diagrams as shown in Fig.8 which are

ξ_W -dependent and satisfy the cutting conditions of Fig.5. We will calculate the contributions of the five cuts of Fig.5 one by one. Firstly we obtain the gauge-parameter-dependent contribution of the first cut of Fig.5 to the real part of W transverse self energy:

$$\begin{aligned} Re\Sigma_{WW}^T(m_W^2)|_{\xi_W-cut} = & -\frac{\alpha^2 m_W^2}{576 s_w^2} \left[3 \sum_{i=u,c} \sum_{j=d,s,b} |V_{ij}|^2 A_{ij} B_{ij} + \sum_{i=e,\mu,\tau} (1-x_i)^2 (2+x_i) \right] \\ & \times (1-\xi_W)(\xi_W^2 - 2\xi_W - 11) \theta[1-\xi_W] - \frac{\alpha^2 m_W^2}{4608} (1-\xi_W)^3 \\ & \times (\xi_W^5 - 3\xi_W^4 - 6\xi_W^3 - 46\xi_W^2 + 165\xi_W + 465) \theta[1-\xi_W]. \end{aligned} \quad (9)$$

Then we obtain the gauge-parameter-dependent contributions of the second and third cuts of Fig.5 to the real part of W transverse self energy:

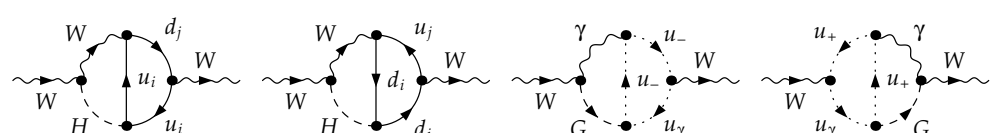
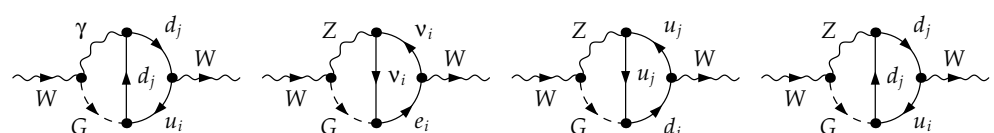
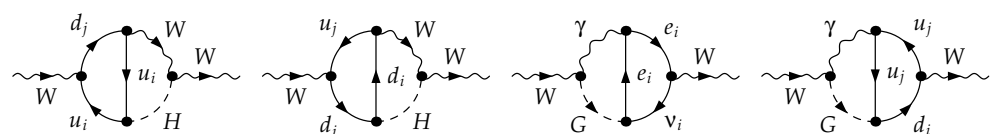
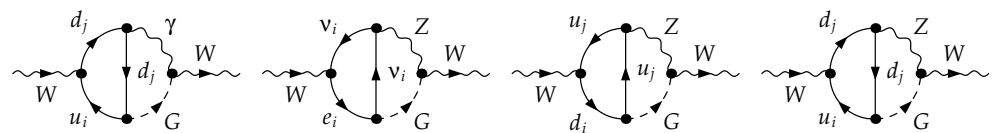
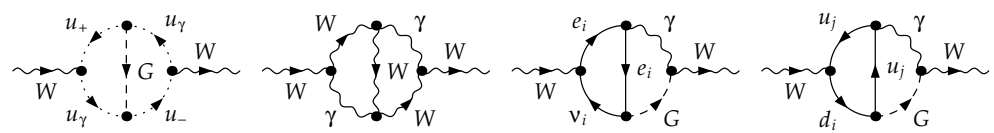
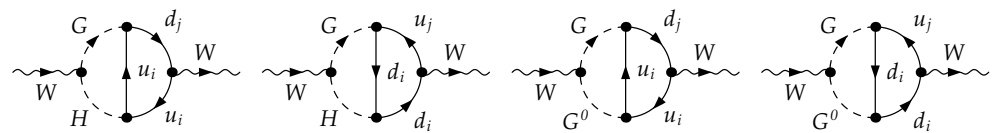
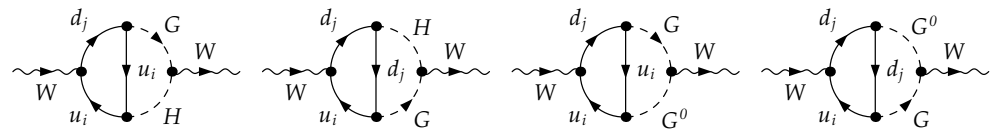
$$\begin{aligned} Re\Sigma_{WW}^T(m_W^2)|_{\xi_W-cut} = & -\frac{\alpha^2 m_W^2}{256 s_w^4} \left[\sum_{i=e,\mu,\tau} \frac{1}{x_i} (1-x_i)(x_i-\xi_W)^2 (x_i^2 + x_i - 2) \theta[m_i - \sqrt{\xi_W} m_W] \right. \\ & + \frac{1}{\xi_W^2} s_w^2 (1-\xi_W)^3 \sum_{i=e,\mu,\tau} x_i (x_i-\xi_W)^2 \theta[\sqrt{\xi_W} m_W - m_i] \theta[1-\xi_W] \\ & + 3 \sum_{i=u,c} \sum_{j=d,s,b} \frac{1}{x_i} |V_{ij}|^2 (\xi_W - x_i + x_j) A_{ij} B_{ij} C_{ij} \theta[m_i - m_j - \sqrt{\xi_W} m_W] \\ & + 3 \sum_{i=u,c} \sum_{j=d,s,b} \frac{1}{x_j} |V_{ij}|^2 (\xi_W - x_j + x_i) A_{ij} B_{ij} C_{ij} \theta[m_j - m_i - \sqrt{\xi_W} m_W] \\ & + \frac{3}{\xi_W^2} s_w^2 (1-\xi_W)^3 \sum_{i=u,c} \sum_{j=d,s,b} |V_{ij}|^2 (\xi_W(x_i + x_j) - (x_i - x_j)^2) C_{ij} \\ & \left. \times \theta[\sqrt{\xi_W} m_W - m_i - m_j] \theta[1-\xi_W] \right]. \end{aligned} \quad (10)$$

Lastly we find the gauge-parameter-dependent contributions of the 4th and 5th cuts of Fig.5 to the real part of W transverse self energy are same as those of the second and the third cuts of Fig.5 (this point can be seen from the symmetries of the four cuts).

Summing up all of the above results we obtain the gauge dependence of the singularities of the real part of W two-loop-level transverse self energy (see Eqs.(6,7,9,10) and the corresponding discussions)

$$\begin{aligned} Re\Sigma_{WW}^T(m_W^2)|_{\xi_W-cut} = & -\frac{\alpha^2 m_W^2}{576 s_w^2} \left[3 \sum_{i=u,c} \sum_{j=d,s,b} |V_{ij}|^2 A_{ij} B_{ij} + \sum_{i=e,\mu,\tau} (1-x_i)^2 (2+x_i) \right] \\ & \times (1-\xi_W)(\xi_W^2 - 2\xi_W - 11) \theta[1-\xi_W]. \end{aligned} \quad (11)$$

From Eq.(5) one finds Eq.(11) is just the gauge dependence of the part containing Heaviside functions of W mass counterterm under the on-shell mass renormalization prescription. So Eq.(11) proves the W mass counterterm of on-shell mass renormalization prescription is gauge dependent.



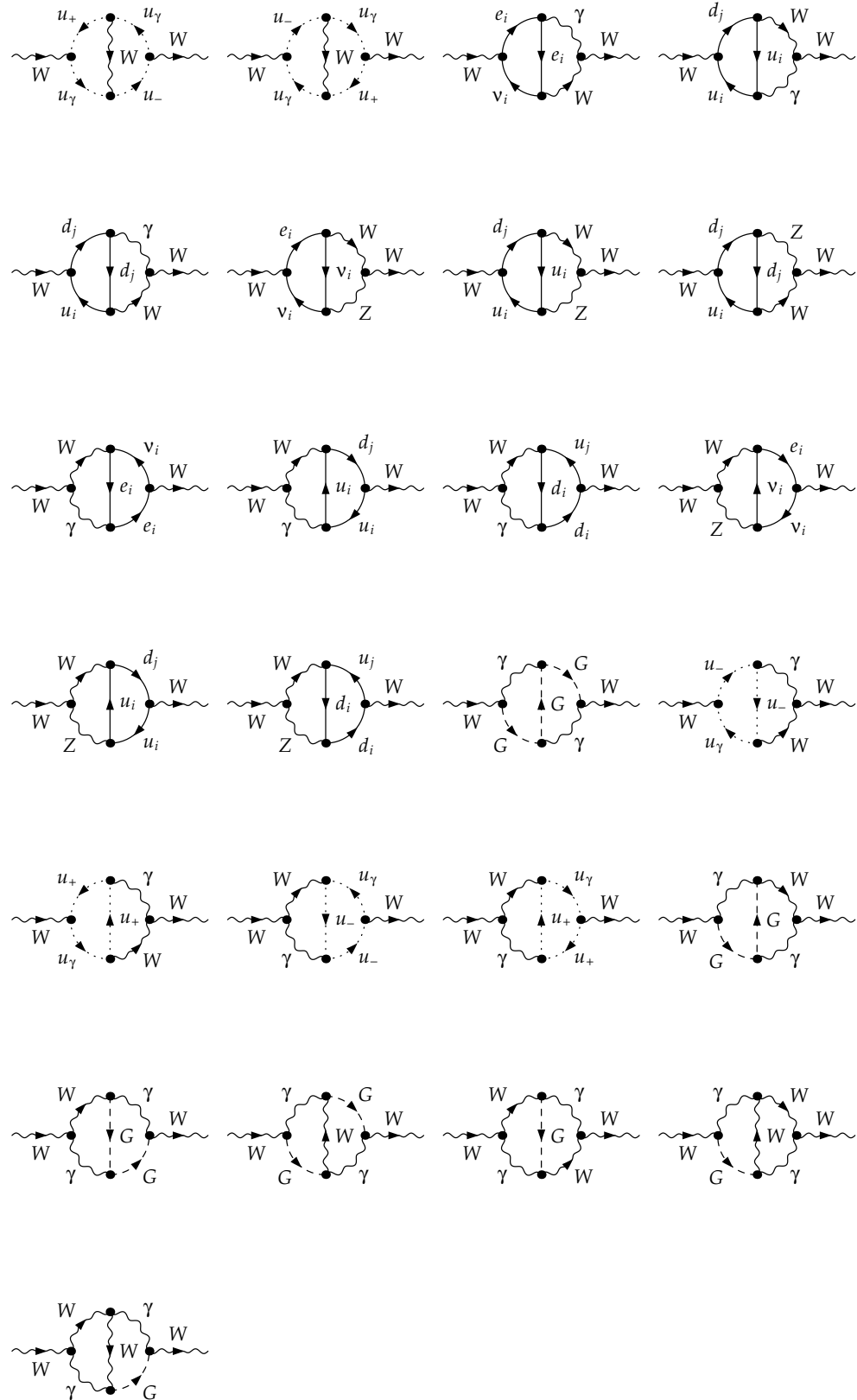


FIG. 8: ξ_W -dependent W self energy diagrams which satisfy the 6th topology of Fig.3 and the cutting conditions of Fig.5.

In order to discuss the gauge dependence of W mass counterterm of the pole mass renormalization prescription we calculate the term (see Eq.(5))

$$m_W \Gamma_W \operatorname{Im} \Sigma_{WW}^{T'}(m_W^2)|_{\xi_W - \text{cut}} = \frac{\alpha^2 m_W^2}{576 s_w^2} \left[3 \sum_{i=u,c} \sum_{j=d,s,b} |V_{ij}|^2 A_{ij} B_{ij} + \sum_{i=e,\mu,\tau} (1-x_i)^2 (2+x_i) \right] \times (1-\xi_W)(\xi_W^2 - 2\xi_W - 11) \theta[1-\xi_W]. \quad (12)$$

Combining Eq.(11) and Eq.(12) one gets (see Eq.(5))

$$\delta m_W^2|_{\xi_W - \text{cut}} = 0 \quad \text{under pole mass renormalization prescription.} \quad (13)$$

This result indicates the part containing Heaviside functions of W mass counterterm of the pole mass renormalization prescription is gauge independent.

B. Gauge dependence of Z mass counterterm under the two mass renormalization prescriptions

Similarly as the case of W gauge boson We only calculate the gauge dependence of the part containing Heaviside function of the real part of Z two-loop-level transverse self energy. The topologies of Z two-loop-level self energy needing calculated have been shown in Fig.3.

For the first topology of Fig.3 only the diagram whose middle propagator (denoted by the broken line) is photon contributes to Z transverse self energy. After careful calculation we obtain the ξ_W -dependent contribution of the cut of the first topology of Fig.3 to the real part of Z transverse self energy

$$\begin{aligned} & \operatorname{Re} \Sigma_{ZZ}^T(m_Z^2)|_{\xi_W - \text{cut}} \\ &= \frac{\alpha^2 m_W^2}{6912 c_w^6 s_w^2} (1-4c_w^2 \xi_W)^{3/2} \left[\frac{3}{c_w^2} (1-4c_w^2 \xi_W)^{3/2} + 8(3(4c_w^2 - 3) \sum_{i=e,\mu,\tau} + 2(8c_w^2 - 5) \sum_{i=u,c} \right. \\ &+ (4c_w^2 - 1) \sum_{i=d,s,b}) \sqrt{1-4c_w^2 x_i} (2c_w^2 x_i + 1) \left. \right] \theta\left[\frac{1}{c_w} - 2\sqrt{\xi_W}\right] + \frac{\alpha^2 m_W^2}{1728 c_w^6} D E \\ &\times \left[\frac{3 s_w^2}{c_w^2} D E - \frac{3}{c_w^2} (1-4c_w^2 \xi_W)^{3/2} - 4(3(4c_w^2 - 3) \sum_{i=e,\mu,\tau} + 2(8c_w^2 - 5) \sum_{i=u,c} + (4c_w^2 - 1) \sum_{i=d,s,b}) \right. \\ &\times \left. \sqrt{1-4c_w^2 x_i} (2c_w^2 x_i + 1) \right] \theta\left[\frac{1}{c_w} - \sqrt{\xi_W} - 1\right], \end{aligned} \quad (14)$$

where m_Z is Z mass, c_w is the cosine of the weak mixing angle, and

$$\begin{aligned} D &= \sqrt{(\xi_W - 1)^2 c_w^4 - 2(\xi_W + 1)c_w^2 + 1}, \\ E &= (\xi_W - 1)^2 c_w^4 - 2(\xi_W - 5)c_w^2 + 1. \end{aligned} \quad (15)$$

For the second topology of Fig.3 there are four Z self-energy diagrams as shown in Fig.9 which satisfy the corresponding cutting condition. By the cutting rules we obtain the ξ_W -dependent

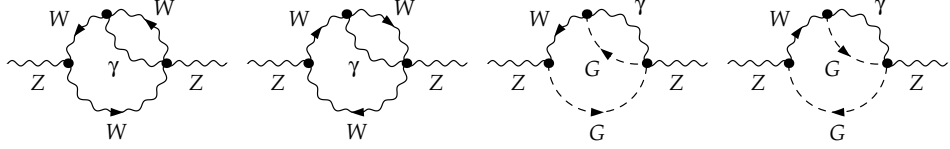


FIG. 9: Z self-energy diagrams which satisfy the second topology of Fig.3 and the corresponding cutting condition.

contribution of the cuts of Fig.9 to the real part of Z transverse self energy :

$$\begin{aligned}
 Re\Sigma_{ZZ}^T(m_Z^2)|_{\xi_W-cut} = & \frac{\alpha^2 m_W^2}{1536 c_w^4} (\xi_W - 1) D [(\xi_W - 1)^3 (\xi_W^3 - \xi_W^2 - 3\xi_W - 33) c_w^6 \\
 & - (\xi_W - 1) (3\xi_W^4 - 9\xi_W^3 - 29\xi_W^2 + 101\xi_W + 366) c_w^4 \\
 & + (3\xi_W^4 - 10\xi_W^3 - 22\xi_W^2 + 170\xi_W - 93) c_w^2 - \xi_W^3 \\
 & + 2\xi_W^2 + 5\xi_W - 18] \theta \left[\frac{1}{c_w} - \sqrt{\xi_W} - 1 \right]. \tag{16}
 \end{aligned}$$

For the third topology of Fig.3 there are also four Z self-energy diagrams as shown in Fig.10 which satisfy the corresponding cutting condition. Obviously Fig.9 and Fig.10 are right-and-left

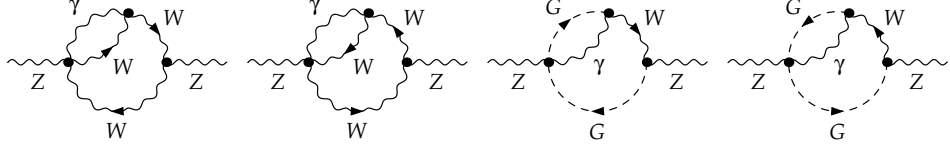


FIG. 10: Z self-energy diagrams which satisfy the third topology of Fig.3 and the corresponding cutting condition.

symmetric. Through calculations we find the ξ_W -dependent contribution of the cuts of Fig.10 to the real part of Z transverse self energy is just equal to that of Fig.9.

For the 4th topology of Fig.3 there are six Z self-energy diagrams as shown in Fig.11 which satisfy the corresponding cutting rules. After careful calculations we obtain the ξ_W -dependent contribution of the cuts of Fig.11 to the real part of Z transverse self energy:

$$\begin{aligned}
 Re\Sigma_{ZZ}^T(m_Z^2)|_{\xi_W-cut} = & \frac{\alpha^2 m_W^2}{4608 c_w^8 s_w^4} (1 - 4 c_w^2 \xi_W)^3 (2c_w^6 - 4c_w^4 + 2c_w^2 - 3) \theta \left[\frac{1}{c_w} - 2\sqrt{\xi_W} \right] \\
 & + \frac{\alpha^2 m_W^2}{2304 c_w^8} [(\xi_W - 1)^6 c_w^{14} - 6(\xi_W - 1)^4 (\xi_W^2 + 11\xi_W + 22) c_w^{12} \\
 & + 3(\xi_W - 1)^2 (12\xi_W^3 + 65\xi_W^2 + 10\xi_W + 201) c_w^{10}
 \end{aligned}$$

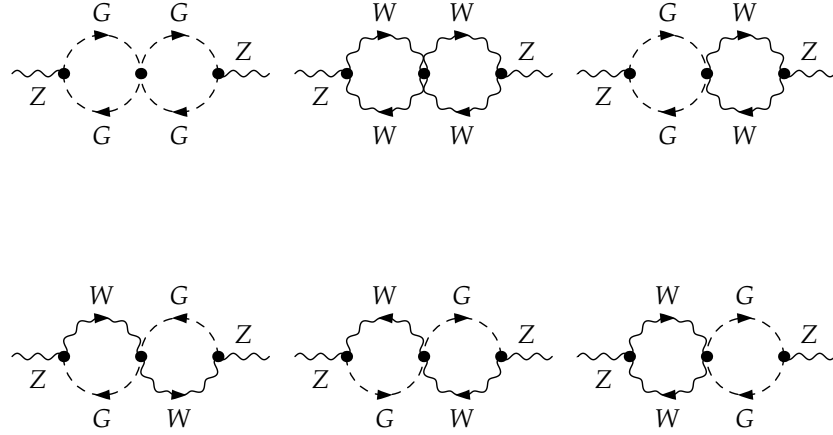
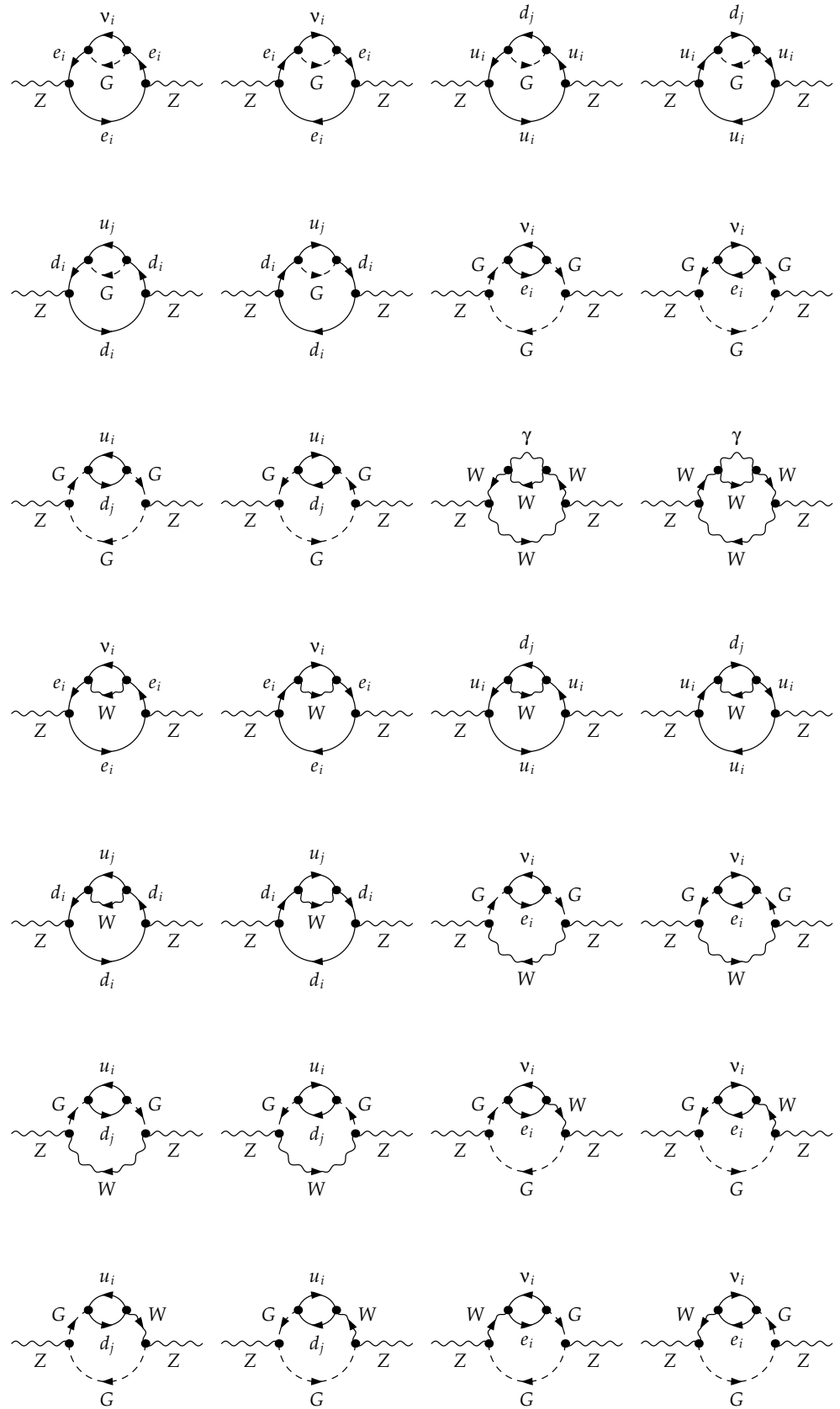


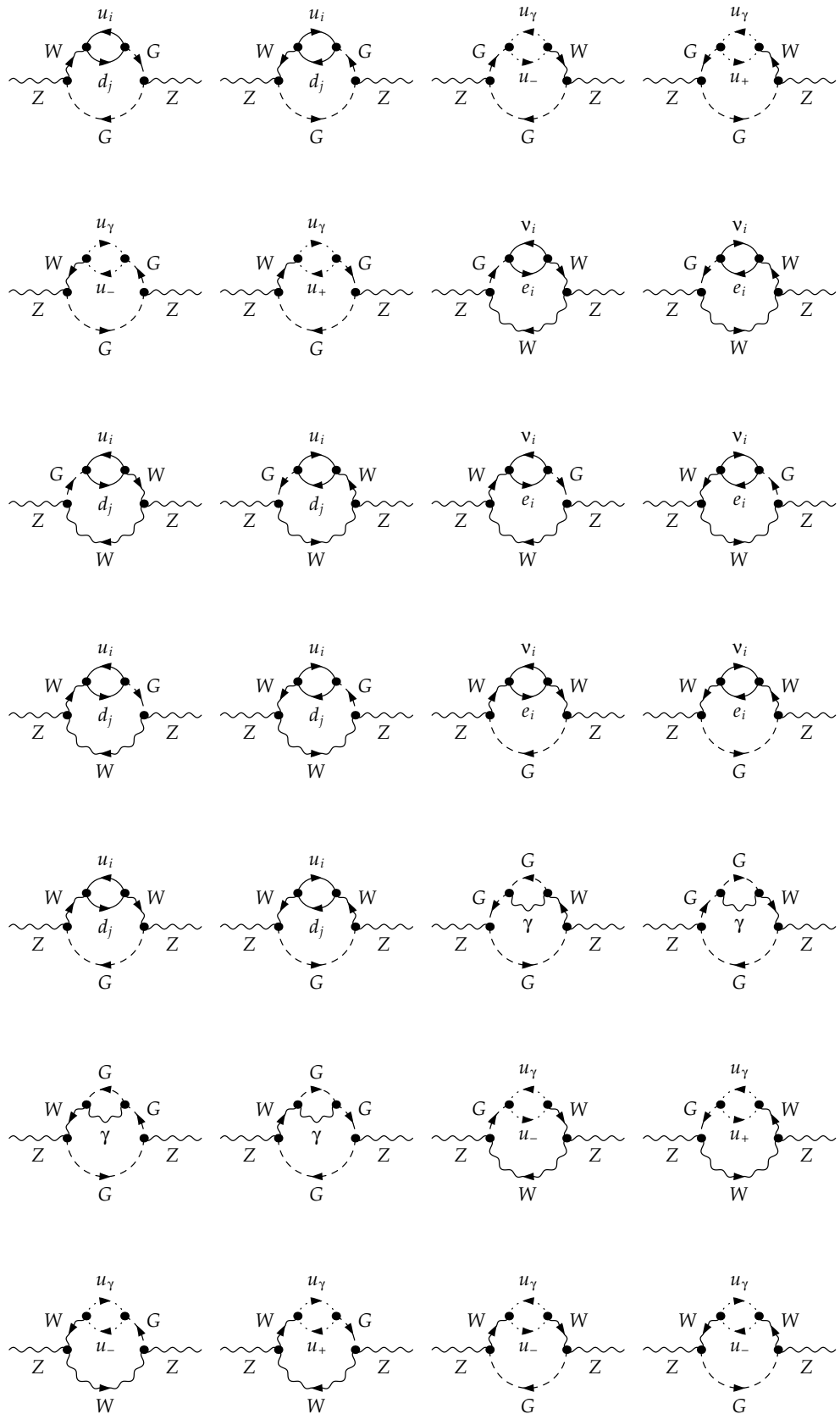
FIG. 11: Z self-energy diagrams which satisfy the 4th topology of Fig.3 and the corresponding cutting condition.

$$\begin{aligned}
& - 2(45\xi_W^4 + 46\xi_W^3 - 228\xi_W^2 - 150\xi_W + 415)c_w^8 \\
& + 3(40\xi_W^3 - 19\xi_W^2 - 98\xi_W + 109)c_w^6 - 6(15\xi_W^2 - 17\xi_W - 12)c_w^4 \\
& + (36\xi_W - 35)c_w^2 - 6] \theta[\frac{1}{c_w} - \sqrt{\xi_W} - 1] - \frac{\alpha^2 m_W^2}{1152 c_w^8 s_w^2} D \sqrt{1 - 4 c_w^2 \xi_W} \\
& \times [4(\xi_W - 1)^2 \xi_W c_w^{10} - (4\xi_w^3 + \xi_W^2 - 38\xi_W + 1)c_w^8 \\
& + 3(4\xi_W^3 + 19\xi_W^2 - 32\xi_W - 3)c_w^6 - 3(9\xi_W^2 - 10\xi_w - 8)c_w^4 \\
& + (18\xi_w - 11)c_w^2 - 3] \theta[\frac{1}{c_w} - \sqrt{\xi_W} - 1]. \quad (17)
\end{aligned}$$

For the 5th topology of Fig.3 there are 84 Z self-energy diagrams as shown in Fig.12 which satisfy the cutting conditions of Fig.4. After careful calculations we obtain the ξ_W -dependent contribution of the cuts of Fig.12 to the real part of Z transverse self energy:

$$\begin{aligned}
& Re \Sigma_{ZZ}^T(m_Z^2)|_{\xi_W-cut} \\
= & \frac{\alpha^2 m_W^2}{192 c_w^2 s_w^2} D E \left[\sum_{i=e,\mu,\tau} (1-x_i)^2 (2+x_i) + 3 \sum_{i=u,c} \sum_{j=d,s,b} |V_{ij}|^2 A_{ij} B_{ij} \right] \theta[\frac{1}{c_w} - \sqrt{\xi_W} - 1] \\
& + \frac{\alpha^2 m_W^2}{64 s_w^4 \xi_W^2} (1 - 4 c_w^2 \xi_W)^{3/2} \sum_{i=e,\mu,\tau} x_i (x_i - \xi_W)^2 \theta[\frac{1}{c_w} - 2\sqrt{\xi_W}] \theta[\sqrt{\xi_W} m_W - m_i] \\
& + \frac{3 \alpha^2 m_W^2}{64 s_w^4 \xi_W^2} (1 - 4 c_w^2 \xi_W)^{3/2} \sum_{i=u,c} \sum_{j=d,s,b} |V_{ij}|^2 C_{ij} (\xi_W (x_i + x_j) - (x_i - x_j)^2) \\
& \times \theta[\frac{1}{c_w} - 2\sqrt{\xi_W}] \theta[\sqrt{\xi_W} m_W - m_i - m_j] - \frac{\alpha^2 m_W^2}{64 c_w^4 s_w^4} (2c_W^2 - 1) \sum_{i=e,\mu,\tau} \frac{1}{x_i} \sqrt{1 - 4 c_w^2 x_i} \\
& \times (x_i - \xi_W)^2 (2c_W^2 - 1 + c_w^2 (4c_W^2 - 5)x_i) \theta[m_i - \sqrt{\xi_W} m_W] \\
& + \frac{\alpha^2 m_W^2}{192 c_w^4 s_w^4} (4c_W^2 - 1) \sum_{i=u,c} \sum_{j=d,s,b} \frac{1}{x_i} |V_{ij}|^2 C_{ij} \sqrt{1 - 4 c_w^2 x_i} (\xi_W - x_i + x_j)
\end{aligned}$$





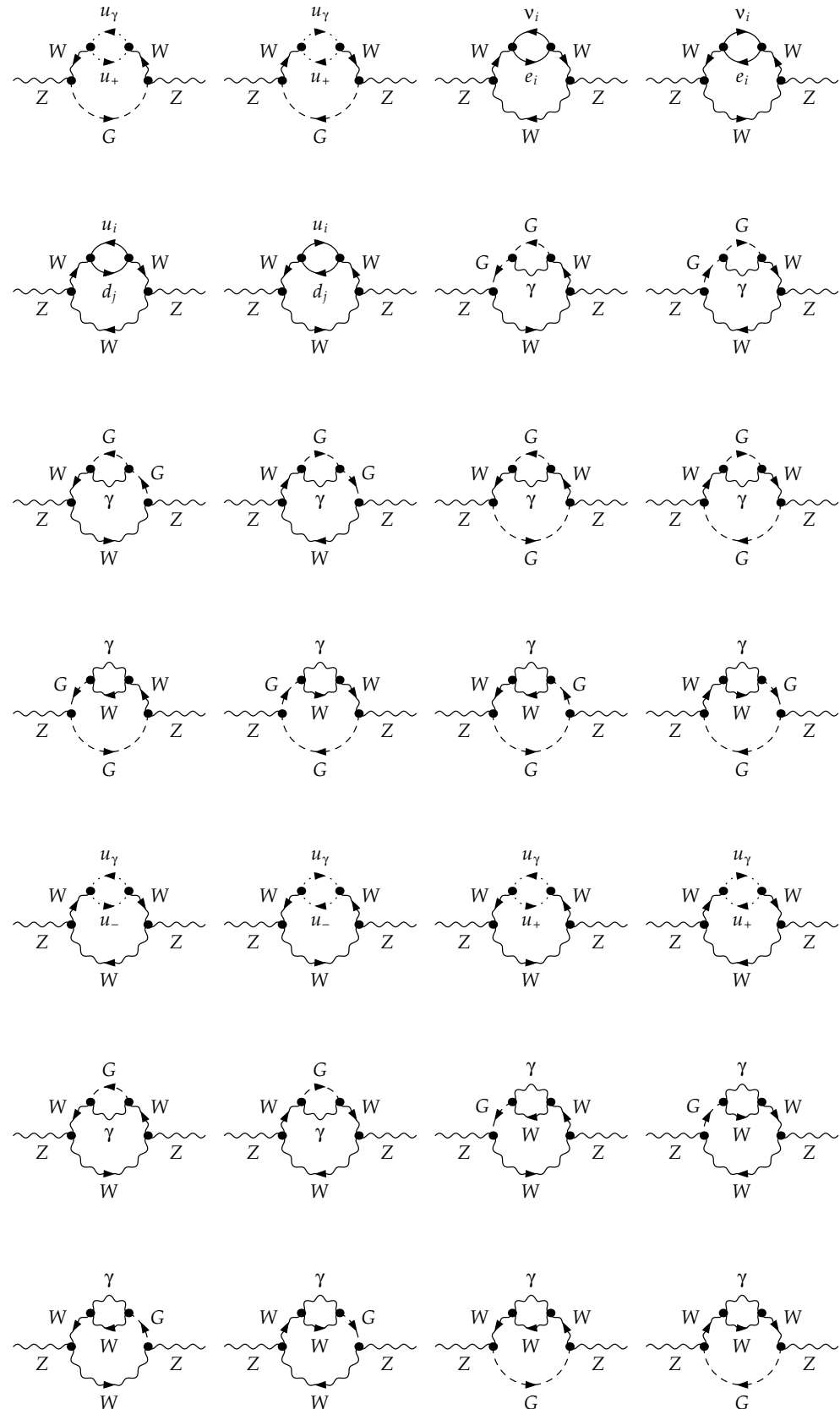


FIG. 12: Z self-energy diagrams which satisfy the 5th topology of Fig.3 and the cutting conditions of Fig.4.

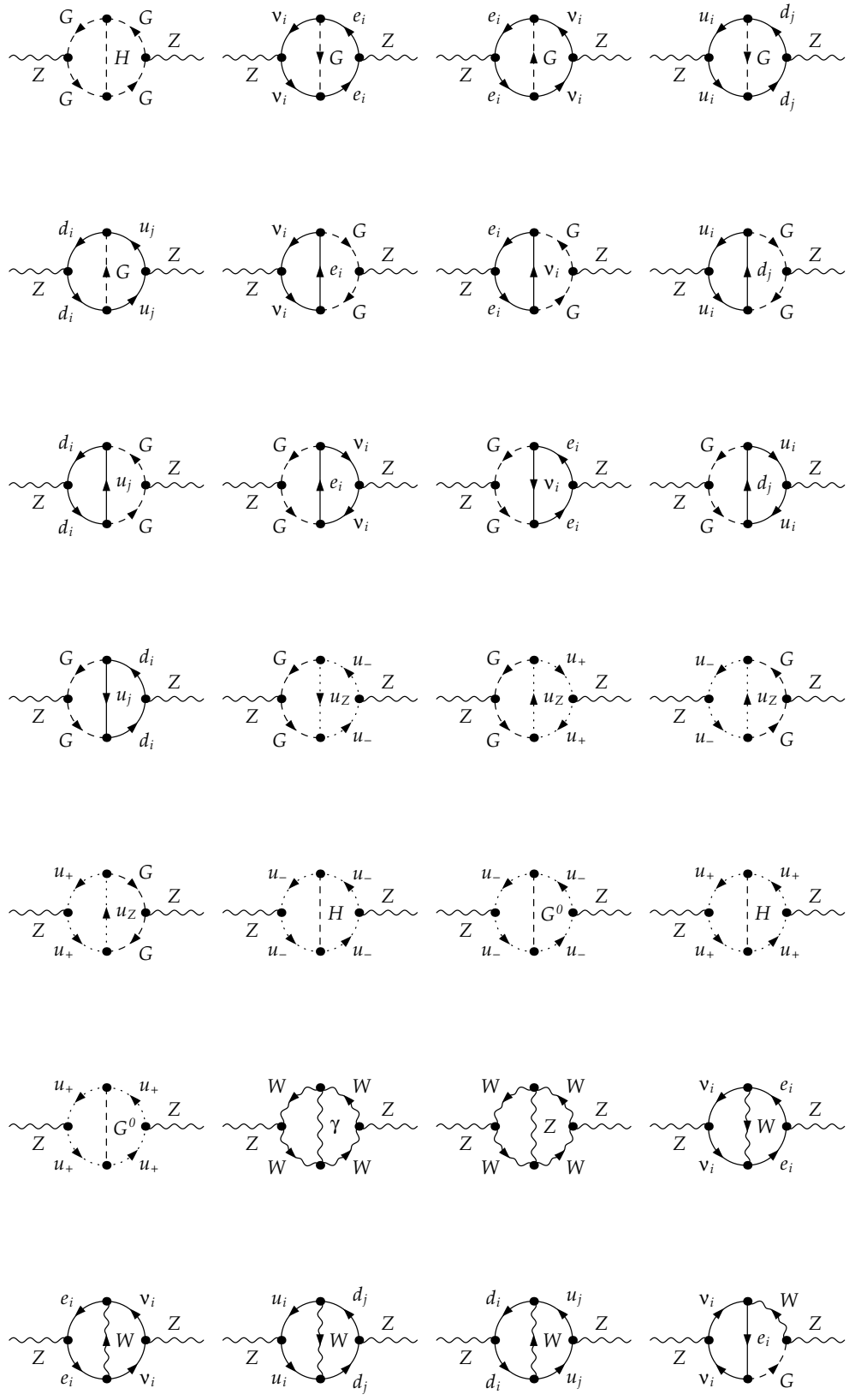
$$\begin{aligned}
& \times (4c_w^2 - 1 + c_w^2(8c_w^2 - 11)x_i) \theta[m_i - m_j - \sqrt{\xi_W}m_W] \\
& + \frac{\alpha^2 m_W^2}{192 c_w^4 s_w^4} (2c_W^2 + 1) \sum_{i=u,c} \sum_{j=d,s,b} \frac{1}{x_j} |V_{ij}|^2 C_{ij} \sqrt{1 - 4c_w^2 x_j} (\xi_W - x_j + x_i) \\
& \times (2c_w^2 + 1 + c_w^2(4c_w^2 - 7)x_j) \theta[m_j - m_i - \sqrt{\xi_W}m_W]. \tag{18}
\end{aligned}$$

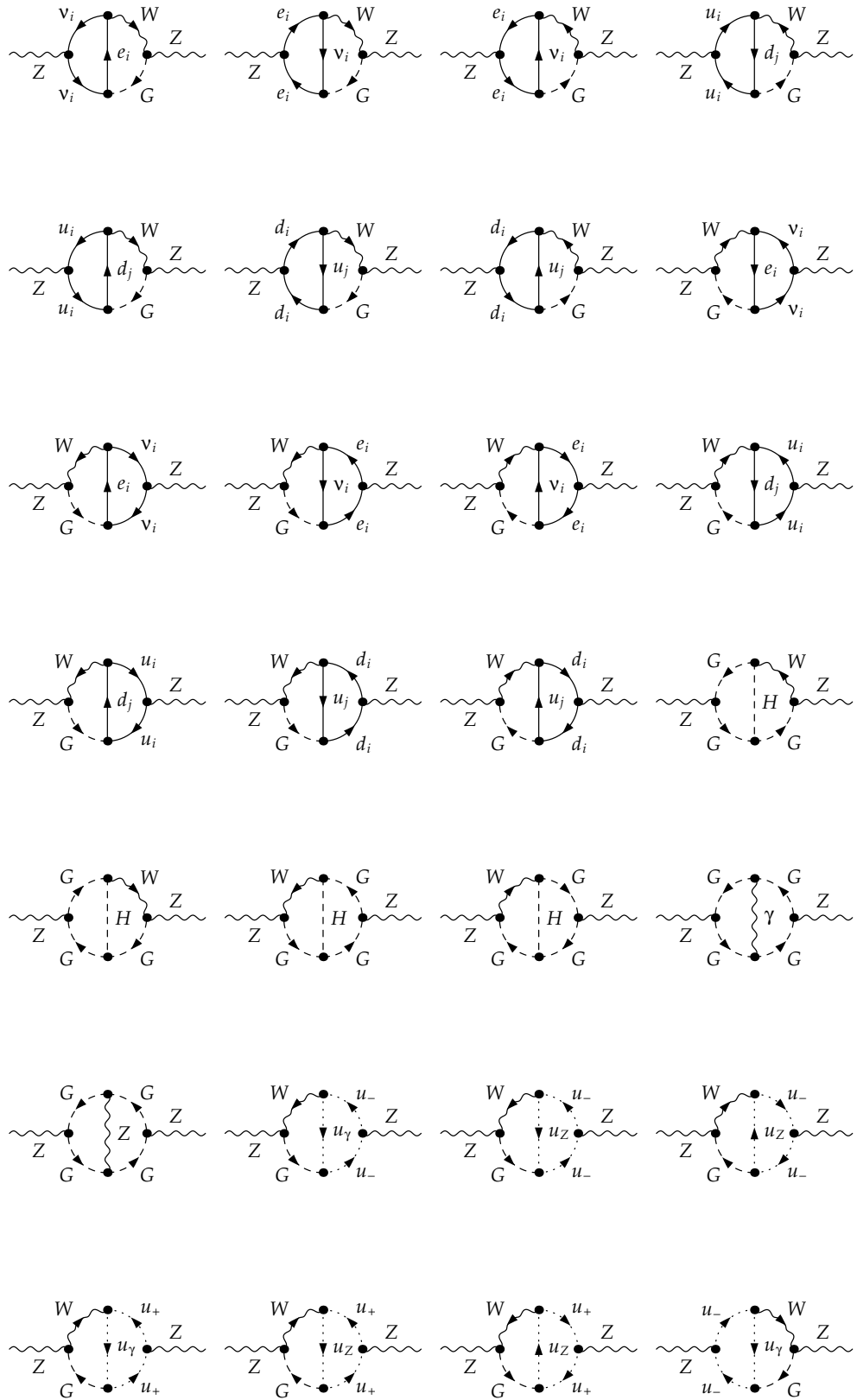
For the 6th topology of Fig.3 there are 124 Z self-energy diagrams as shown in Fig.13 which are ξ_W dependent and satisfy the cutting conditions of Fig.5. We will calculate the contributions of the five cuts of Fig.5 one by one. Firstly we obtain the ξ_W -dependent contribution of the first cut of Fig.5 to the real part of Z transverse self energy:

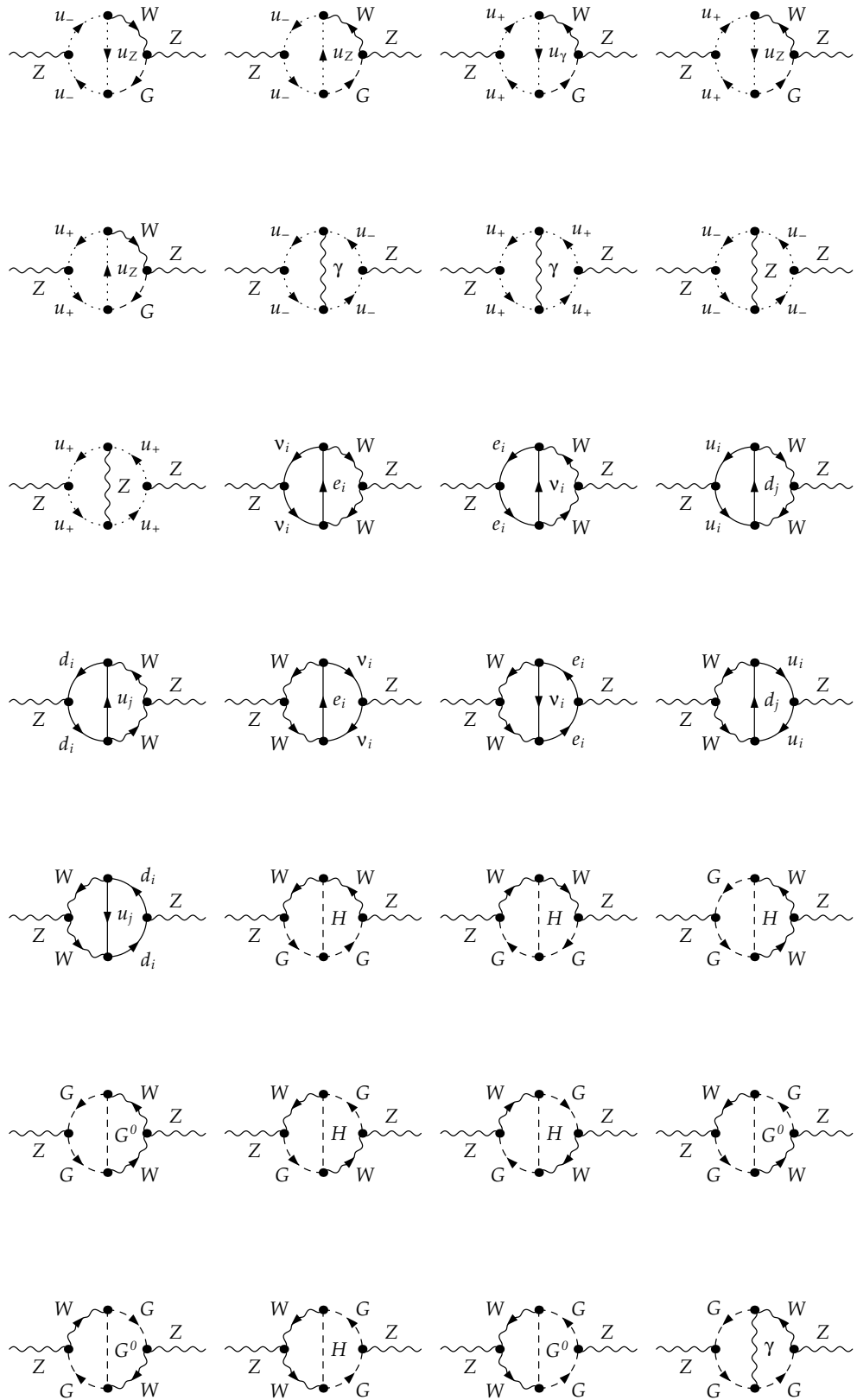
$$\begin{aligned}
Re\Sigma_{ZZ}^T(m_Z^2)|_{\xi_W-cut} = & \frac{\alpha^2 m_W^2}{4608 c_w^8 s_w^4} (1 - 4c_w^2 \xi_W)^3 (1 + 4c_w^4 - 2c_w^6) \theta\left[\frac{1}{c_w} - 2\sqrt{\xi_W}\right] \\
& - \frac{\alpha^2 m_W^2}{576 c_w^6 s_w^4} (1 - 4c_w^2 \xi_W)^{3/2} [3 + \left(\sum_{i=e,\mu,\tau} 2c_w^2 - 1 + c_w^2(4c_w^2 - 5)x_i\right. \\
& + \left.\sum_{i=u,c} 4c_w^2 - 1 + c_w^2(8c_w^2 - 11)x_i + \sum_{i=d,s,b} 2c_w^2 + 1 + c_w^2(4c_W^2 - 7)x_i\right) \\
& \times \sqrt{1 - 4c_w^2 x_i}] \theta\left[\frac{1}{c_w} - 2\sqrt{\xi_W}\right] + \frac{\alpha^2 m_W^2}{1152 c_w^8 s_w^2} D \sqrt{1 - 4c_w^2 \xi_W} \\
& \times [4(\xi_W - 1)^2 \xi_W c_w^{10} + (4\xi_W^3 - 17\xi_W^2 + 46\xi_W - 1)c_w^8 \\
& + (4\xi_W^3 + 55\xi_W^2 - 20\xi_W - 11)c_w^6 - (9\xi_W^2 + 42\xi_W - 6)c_w^4 \\
& + (6\xi_W + 7)c_w^2 - 1] \theta\left[\frac{1}{c_w} - \sqrt{\xi_W} - 1\right] \\
& + \frac{\alpha^2 m_W^2}{2304 c_w^8} [3(\xi_W - 1)^6 c_w^{14} + 2(\xi_W - 1)^4 (\xi_W^2 + 25\xi_W + 100)c_w^{12} \\
& - 3(\xi_W - 1)^2 (4\xi_W^3 + 85\xi_W^2 + 58\xi_W + 141)c_w^{10} \\
& + 6(5\xi_W^4 + 74\xi_W^3 - 144\xi_W^2 - 50\xi_W - 13)c_w^8 \\
& - (40\xi_W^3 + 411\xi_W^2 - 798\xi_W - 581)c_w^6 + 6(5\xi_W^2 + 31\xi_W - 42)c_w^4 \\
& - 3(4\xi_W + 11)c_w^2 + 2] \theta\left[\frac{1}{c_w} - \sqrt{\xi_W} - 1\right] + \frac{\alpha^2 m_W^2}{288 c_w^6 s_w^2} D E \\
& \times [3 + \left(\sum_{i=e,\mu,\tau} (2c_w^2 - 1 + c_w^2(4c_w^2 - 5)x_i) + \sum_{i=u,c} (4c_w^2 - 1 + c_w^2(8c_w^2 - 11)x_i)\right. \\
& \left.+ \sum_{i=d,s,b} (2c_w^2 + 1 + c_w^2(4c_W^2 - 7)x_i)\right) \sqrt{1 - 4c_w^2 x_i}] \theta\left[\frac{1}{c_w} - \sqrt{\xi_W} - 1\right]. \tag{19}
\end{aligned}$$

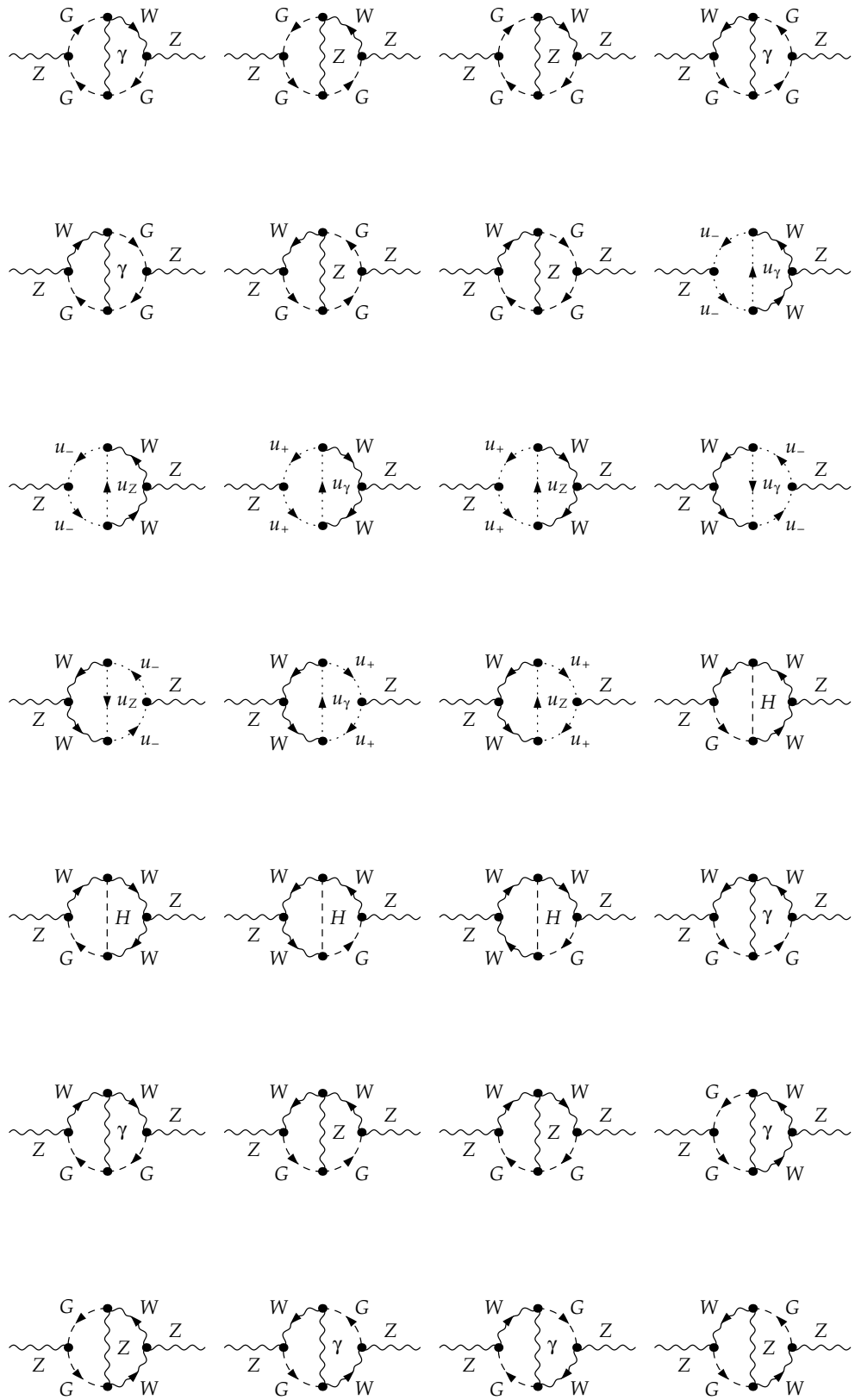
Then we obtain the ξ_W -dependent contribution of the second and third cuts of Fig.5 to the real part of Z transverse self energy:

$$\begin{aligned}
& Re\Sigma_{ZZ}^T(m_Z^2)|_{\xi_W-cut} \\
& = -\frac{\alpha^2 m_W^2}{384 c_w^2 s_w^2} D E \left[\sum_{i=e,\mu,\tau} (1 - x_i)^2 (2 + x_i) + 3 \sum_{i=u,c} \sum_{j=d,s,b} |V_{ij}|^2 A_{ij} B_{ij} \right] \theta\left[\frac{1}{c_w} - \sqrt{\xi_W} - 1\right]
\end{aligned}$$









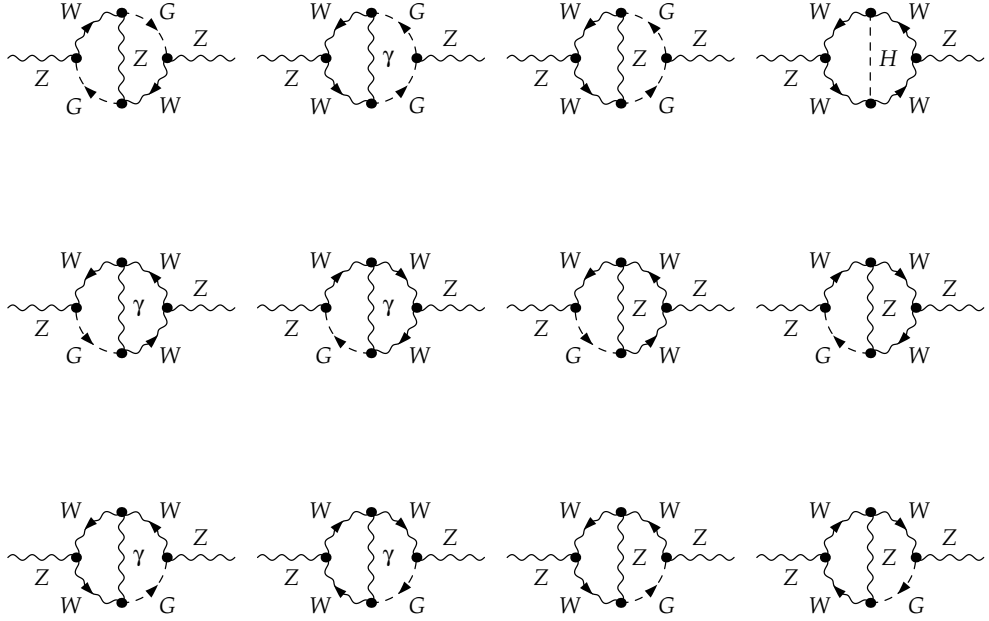


FIG. 13: ξ_W -dependent Z self-energy diagrams which satisfy the 6th topology of Fig.3 and the cutting conditions of Fig.5.

$$\begin{aligned}
& - \frac{\alpha^2 m_W^2}{1536 c_w^4} (\xi_W - 1) D [(\xi_W - 1)^3 (\xi_W^3 - \xi_W^2 - 3\xi_W - 33) c_w^6 \\
& - (\xi_W - 1)(3\xi_W^4 - 9\xi_W^3 - 29\xi_W^2 + 101\xi_W + 366) c_w^4 \\
& + (3\xi_W^4 - 10\xi_W^3 - 22\xi_W^2 + 170\xi_W - 93) c_w^2 - \xi_W^3 + 2\xi_W^2 + 5\xi_W - 18] \theta \left[\frac{1}{c_w} - \sqrt{\xi_W} - 1 \right] \\
& - \frac{\alpha^2 m_W^2}{128 s_w^4 \xi_W^2} (1 - 4 c_w^2 \xi_W)^{3/2} \sum_{i=e,\mu,\tau} x_i (x_i - \xi_W)^2 \theta \left[\frac{1}{c_w} - 2\sqrt{\xi_W} \right] \theta [\sqrt{\xi_W} m_W - m_i] \\
& - \frac{3 \alpha^2 m_W^2}{128 s_w^4 \xi_W^2} (1 - 4 c_w^2 \xi_W)^{3/2} \sum_{i=u,c} \sum_{j=d,s,b} |V_{ij}|^2 C_{ij} (\xi_W (x_i + x_j) - (x_i - x_j)^2) \\
& \times \theta \left[\frac{1}{c_w} - 2\sqrt{\xi_W} \right] \theta [\sqrt{\xi_W} m_W - m_i - m_j] + \frac{\alpha^2 m_W^2}{128 c_w^4 s_w^4} (2c_W^2 - 1) \\
& \times \sum_{i=e,\mu,\tau} \frac{1}{x_i} \sqrt{1 - 4 c_w^2 x_i} (x_i - \xi_W)^2 (2c_W^2 - 1 + c_w^2 (4c_W^2 - 5)x_i) \theta [m_i - \sqrt{\xi_W} m_W] \\
& - \frac{\alpha^2 m_W^2}{384 c_w^4 s_w^4} (4c_W^2 - 1) \sum_{i=u,c} \sum_{j=d,s,b} \frac{1}{x_i} |V_{ij}|^2 C_{ij} \sqrt{1 - 4 c_w^2 x_i} (\xi_W - x_i + x_j) \\
& \times (4c_W^2 - 1 + c_w^2 (8c_W^2 - 11)x_i) \theta [m_i - m_j - \sqrt{\xi_W} m_W] \\
& - \frac{\alpha^2 m_W^2}{384 c_w^4 s_w^4} (2c_W^2 + 1) \sum_{i=u,c} \sum_{j=d,s,b} \frac{1}{x_j} |V_{ij}|^2 C_{ij} \sqrt{1 - 4 c_w^2 x_j} (\xi_W - x_j + x_i) \\
& \times (2c_W^2 + 1 + c_w^2 (4c_W^2 - 7)x_j) \theta [m_j - m_i - \sqrt{\xi_W} m_W]. \tag{20}
\end{aligned}$$

From Fig.5 one readily sees the 4th and 5th cuts are right-and-left symmetric with the second and

third cuts. After careful calculations we also find the ξ_W -dependent contribution of the 4th and 5th cuts of Fig.5 to the real part of Z transverse self energy is equal to that of the second and third cuts of Fig.5.

Summing up all of the above results we obtain the gauge dependence of the part containing Heaviside functions of the real part of Z two-loop-level transverse self energy (see Eqs.(14-20) and the corresponding discussions)

$$\begin{aligned}
& Re \Sigma_{ZZ}^T(m_Z^2)|_{\xi_W-cut} \\
= & \frac{\alpha^2 m_W^2}{1728 c_w^6 s_w^2} \left[9 + 3 \sum_{i=e,\mu,\tau} \sqrt{1 - 4 c_w^2 x_i} (16x_i c_w^6 + (8 - 24x_i)c_w^4 + (7x_i - 12)c_w^2 + 5) \right. \\
+ & \sum_{i=u,c} \sqrt{1 - 4 c_w^2 x_i} (64x_i c_w^6 + (32 - 80x_i)c_w^4 + (7x_i - 40)c_w^2 + 17) \\
+ & \left. \sum_{i=d,s,b} \sqrt{1 - 4 c_w^2 x_i} (16x_i c_w^6 + 8(1 - x_i)c_w^4 - (17x_i + 4)c_w^2 + 5) \right] \\
\times & [2D E \theta\left[\frac{1}{c_w} - \sqrt{\xi_W} - 1\right] - \frac{1}{s_w^2} (1 - 4 c_w^2 \xi_W)^{3/2} \theta\left[\frac{1}{c_w} - 2\sqrt{\xi_W}\right]]. \tag{21}
\end{aligned}$$

This result proves that the part containing Heaviside functions of Z mass counterterm is gauge dependent under the on-shell mass renormalization prescription, i.e. the Z mass counterterm is gauge dependent under the on-shell mass renormalization prescription.

In order to calculate the gauge dependence of Z mass definition of the pole mass renormalization prescription we need to calculate the following term (see Eq.(5)):

$$\begin{aligned}
& m_Z \Gamma_Z Im \Sigma_{ZZ}^{T'}(m_Z^2)|_{\xi_W-cut} \\
= & \frac{\alpha^2 m_W^2}{1728 c_w^6 s_w^2} \left[9 + 3 \sum_{i=e,\mu,\tau} \sqrt{1 - 4 c_w^2 x_i} (16x_i c_w^6 + (8 - 24x_i)c_w^4 + (7x_i - 12)c_w^2 + 5) \right. \\
+ & \sum_{i=u,c} \sqrt{1 - 4 c_w^2 x_i} (64x_i c_w^6 + (32 - 80x_i)c_w^4 + (7x_i - 40)c_w^2 + 17) \\
+ & \left. \sum_{i=d,s,b} \sqrt{1 - 4 c_w^2 x_i} (16x_i c_w^6 + 8(1 - x_i)c_w^4 - (17x_i + 4)c_w^2 + 5) \right] \\
\times & \left[\frac{1}{s_w^2} (1 - 4 c_w^2 \xi_W)^{3/2} \theta\left[\frac{1}{c_w} - 2\sqrt{\xi_W}\right] - 2D E \theta\left[\frac{1}{c_w} - \sqrt{\xi_W} - 1\right] \right]. \tag{22}
\end{aligned}$$

From Eq.(5) and Eqs.(21,22) we get the gauge dependence of the part containing Heaviside functions of Z mass counterterm under the pole mass renormalization prescription:

$$\delta m_Z^2|_{\xi_W-cut} = 0 \quad \text{under pole mass renormalization prescription.} \tag{23}$$

C. Gauge dependence of the counterterm of the sine of the weak mixing angle under the two mass renormalization prescriptions

From the two-loop-level W and Z's mass counterterms we can calculate the two-loop-level counterterm of the sine of the weak mixing angle. To two-loop level one has [2]

$$\delta s_w = \frac{c_w^2}{2s_w} \left(\frac{\delta m_Z^2}{m_Z^2} - \frac{\delta m_W^2}{m_W^2} \right) + \frac{c_w^2}{2s_w} \left(\frac{\delta m_Z^2 \delta m_W^2}{m_Z^2 m_W^2} - \frac{(\delta m_Z^2)^2}{m_Z^4} \right) - \frac{c_w^4}{8s_w^3} \left(\frac{\delta m_Z^2}{m_Z^2} - \frac{\delta m_W^2}{m_W^2} \right)^2 + O(g^6). \quad (24)$$

The one-loop-level W and Z's mass counterterms have been proven gauge independent [6]. So we only need to calculate the gauge dependence of the first term of the r.h.s. of Eq.(24). From Eqs.(11,21) we obtain the gauge dependence of the part containing Heaviside functions of the two-loop-level δs_w under the on-shell mass renormalization prescription

$$\begin{aligned} \delta s_w|_{\xi_W-cut} = & \frac{\alpha^2}{3456 c_w^2 s_w^3} \left[9 + 3 \sum_{i=e,\mu,\tau} \sqrt{1 - 4 c_w^2 x_i} (16x_i c_w^6 + (8 - 24x_i)c_w^4 + (7x_i - 12)c_w^2 + 5) \right. \\ & + \sum_{i=u,c} \sqrt{1 - 4 c_w^2 x_i} (64x_i c_w^6 + (32 - 80x_i)c_w^4 + (7x_i - 40)c_w^2 + 17) \\ & + \sum_{i=d,s,b} \sqrt{1 - 4 c_w^2 x_i} (16x_i c_w^6 + 8(1 - x_i)c_w^4 - (17x_i + 4)c_w^2 + 5) \Big] \\ & \times [2D E \theta \left(\frac{1}{c_w} - \sqrt{\xi_W} - 1 \right) - \frac{1}{s_w^2} (1 - 4 c_w^2 \xi_W)^{3/2} \theta \left(\frac{1}{c_w} - 2\sqrt{\xi_W} \right)] \\ & + \frac{\alpha^2 c_w^2}{1152 s_w^3} \left[3 \sum_{i=u,c} \sum_{j=d,s,b} |V_{ij}|^2 A_{ij} B_{ij} + \sum_{i=e,\mu,\tau} (1 - x_i)^2 (2 + x_i) \right] \\ & \times (1 - \xi_W)(\xi_W^2 - 2\xi_W - 11) \theta[1 - \xi_W] \quad \text{under on-shell prescription.} \quad (25) \end{aligned}$$

Eq.(25) implies δs_w is gauge dependent under the on-shell mass renormalization prescription. On the other hand, from Eqs.(13,23) we obtain the gauge dependence of the part containing Heaviside functions of the two-loop-level δs_w under the pole mass renormalization prescription

$$\delta s_w|_{\xi_W-cut} = 0 \quad \text{under pole prescription.} \quad (26)$$

III. GAUGE DEPENDENCE OF PHYSICAL RESULT UNDER THE ON-SHELL AND POLE MASS RENORMALIZATION PRESCRIPTIONS

From the results of section II we have found the counterterms of W and Z's mass and the sine of the weak mixing angle are gauge dependent under the on-shell mass renormalization prescription, but those gauge dependencies don't appear in the counterterms of the pole mass renormalization prescription. Maybe this conclusion is not enough to judge which renormalization prescription is reasonable, since in some cases the physical parameter's counterterm is gauge dependent. So we

should judge the reasonableness of the renormalization prescriptions from the gauge independence of physical result.

For example we calculate the gauge dependence of the two-loop-level cross section of the physical process $\mu \rightarrow \nu_\mu e^- \bar{\nu}_e$ under the two mass renormalization prescriptions. Note that we only calculate the gauge dependence of the part containing the Heaviside functions $\theta[1 - \xi_W]$, $\theta[1/c_w - \sqrt{\xi_W} - 1]$ and $\theta[1/c_w - 2\sqrt{\xi_W}]$ of the cross section of the physical process. This will not affect our conclusion. Under this consideration only the diagrams containing the two-loop-level counterterms δs_w and δm_W^2 as shown in Fig.14 need to be calculated. This is because: 1) all of the one-loop-level physical

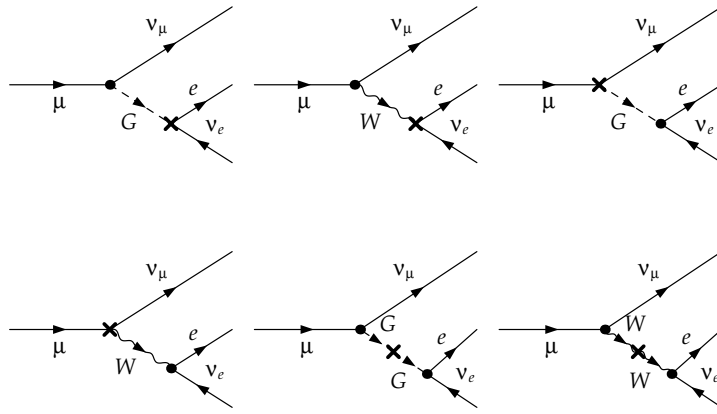


FIG. 14: Diagrams of $\mu \rightarrow \nu_\mu e^- \bar{\nu}_e$ containing the two-loop-level counterterms δs_w and δm_W^2 .

parameter's counterterms and the two-loop-level counterterms of the lepton masses and electron charge don't contain the Heaviside functions $\theta[1 - \xi_W]$, $\theta[1/c_w - \sqrt{\xi_W} - 1]$ and $\theta[1/c_w - 2\sqrt{\xi_W}]$; 2) the energy of the incoming particle of this process is order of muon energy which doesn't reach the threshold of the singularities containing the Heaviside functions $\theta[1 - \xi_W]$, $\theta[1/c_w - \sqrt{\xi_W} - 1]$ and $\theta[1/c_w - 2\sqrt{\xi_W}]$, thus all of loop momentum integrals of the Feynman diagrams don't contribute to these Heaviside functions. We can easily get the contribution of Fig.14 to the physical amplitude $\mu \rightarrow \nu_\mu e^- \bar{\nu}_e$

$$\begin{aligned} \mathcal{M}(\mu \rightarrow \nu_\mu e^- \bar{\nu}_e) \rightarrow & \frac{4\pi\alpha(m_e m_\mu F_1 - m_W^2 F_2)}{m_W^2 s_w^3 (m_W^2 - m_e^2 - 2q_2 \cdot q_3)} \delta s_w + \frac{2\pi\alpha \delta m_W^2}{m_W^4 s_w^2 (m_W^2 - m_e^2 - 2q_2 \cdot q_3)^2} \\ & \times [m_e m_\mu (2m_W^2 - m_e^2 - 2q_2 \cdot q_3) F_1 - m_W^4 F_2], \end{aligned} \quad (27)$$

where m_e and m_μ is the mass of electron and muon, q_2 and q_3 are the momentums of electron and the anti electron neutrino, and

$$F_1 = \bar{u}(q_1) \gamma_R u(p) \bar{u}(q_2) \gamma_L \nu(q_3), \quad F_2 = \bar{u}(q_1) \gamma^\mu \gamma_L u(p) \bar{u}(q_2) \gamma_\mu \gamma_L \nu(q_3), \quad (28)$$

where p and q_1 are the momentums of muon and muon neutrino, and γ_L and γ_R are the left- and right- handed helicity operators. The contribution of Eq.(27) to the two-loop-level cross section of $\mu \rightarrow \nu_\mu e^- \bar{\nu}_e$ is

$$\begin{aligned} \sigma(\mu \rightarrow \nu_\mu e^- \bar{\nu}_e) &\propto |\mathcal{M}(\mu \rightarrow \nu_\mu e^- \bar{\nu}_e)|^2 \\ &\rightarrow \frac{16\pi^2\alpha^2 q_1 \cdot q_2 (m_e^2 - m_\mu^2 + 2q_1 \cdot q_2)}{m_W^4 s_w^4} \left(\frac{2\delta s_w}{s_w} + \frac{\delta m_W^2}{m_W^2} \right). \end{aligned} \quad (29)$$

In Eq.(29) we have averaged the result over the incoming fermion's helicity states and summed up the results for the different outgoing fermions' helicity states. On the other hand we only keep the lowest order of the quantities m_e^2/m_W^2 , m_μ^2/m_W^2 and so on in Eq.(29), since the energies of the external-line particles are very small compared with m_W^2 .

From Eqs.(11,25) and Eq.(29) we obtain the gauge dependence of the part containing the Heaviside functions $\theta[1 - \xi_W]$, $\theta[1/c_w - \sqrt{\xi_W} - 1]$ and $\theta[1/c_w - 2\sqrt{\xi_W}]$ of the two-loop-level cross section of $\mu \rightarrow \nu_\mu e^- \bar{\nu}_e$ under the on-shell mass renormalization prescription

$$\begin{aligned} \sigma_2(\mu \rightarrow \nu_\mu e^- \bar{\nu}_e)_{\xi_W-cut} &\rightarrow \frac{\pi^2\alpha^4 q_1 \cdot q_2 (m_e^2 - m_\mu^2 + 2q_1 \cdot q_2)}{108m_W^4 c_w^2 s_w^8} \left[9 \right. \\ &+ 3 \sum_{i=e,\mu,\tau} \sqrt{1 - 4c_w^2 x_i} (16x_i c_w^6 + (8 - 24x_i)c_w^4 + (7x_i - 12)c_w^2 + 5) \\ &+ \sum_{i=u,c} \sqrt{1 - 4c_w^2 x_i} (64x_i c_w^6 + (32 - 80x_i)c_w^4 + (7x_i - 40)c_w^2 + 17) \\ &+ \left. \sum_{i=d,s,b} \sqrt{1 - 4c_w^2 x_i} (16x_i c_w^6 + 8(1 - x_i)c_w^4 - (17x_i + 4)c_w^2 + 5) \right] \\ &\times [2D E \theta\left[\frac{1}{c_w} - \sqrt{\xi_W} - 1\right] - \frac{1}{s_w^2} (1 - 4c_w^2 \xi_W)^{3/2} \theta\left[\frac{1}{c_w} - 2\sqrt{\xi_W}\right]] \\ &+ \frac{\pi^2\alpha^4 q_1 \cdot q_2 (m_e^2 - m_\mu^2 + 2q_1 \cdot q_2)}{36m_W^4 s_w^8} (2c_w^2 - 1)(1 - \xi_W)(\xi_W^2 - 2\xi_W - 11) \\ &\times \left[3 \sum_{i=u,c} \sum_{j=d,s,b} |V_{ij}|^2 A_{ij} B_{ij} + \sum_{i=e,\mu,\tau} (1 - x_i)^2 (2 + x_i) \right] \theta[1 - \xi_W]. \end{aligned} \quad (30)$$

Eq.(30) implies the on-shell mass renormalization prescription makes the cross section of the physical process $\mu \rightarrow \nu_\mu e^- \bar{\nu}_e$ gauge dependent. So the on-shell mass renormalization prescription is a wrong mass renormalization prescription beyond one-loop level. The quantitative order of this gauge dependence can be seen in Fig.15. In Fig.15 the following data have been used: $e = 0.3028$, $s_w^2 = 0.2312$, $m_W = 80.42\text{Gev}$, $m_u = 3\text{Mev}$, $m_c = 1.25\text{Gev}$, $m_t = 174.3\text{Gev}$, $m_d = 6\text{Mev}$, $m_s = 120\text{Mev}$, $m_b = 4.2\text{Gev}$, $m_e = 0.5110\text{Mev}$, $m_\mu = 105.7\text{Mev}$, $m_\tau = 1.777\text{Gev}$, $|V_{ud}| = 0.975$, $|V_{us}| = 0.223$, $|V_{ub}| = 0.004$, $|V_{cd}| = 0.222$, $|V_{cs}| = 0.974$, $|V_{cb}| = 0.040$, $|V_{td}| = 0.009$, $|V_{ts}| = 0.039$, and $|V_{tb}| = 0.999$ [13]. Obviously the gauge dependence of $\sigma(\mu \rightarrow \nu_\mu e^- \bar{\nu}_e)$ induced by the on-shell mass renormalization prescription can not be neglected at the two-loop level. On the other hand,

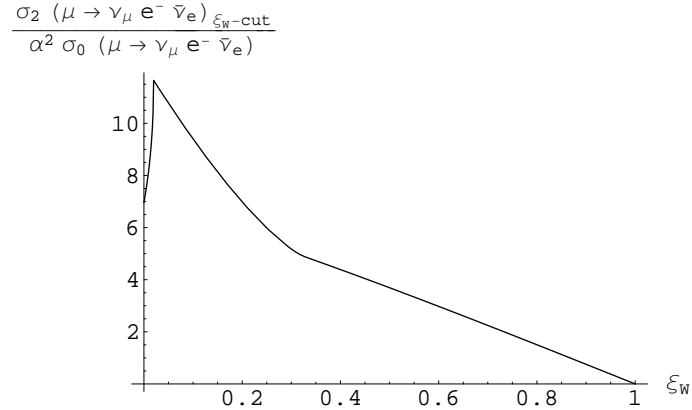


FIG. 15: Gauge dependence of the two-loop-level cross section of $\mu \rightarrow \nu_\mu e^- \bar{\nu}_e$ under the on-shell mass renormalization prescription, where $q_1 \cdot q_2 = q_2 \cdot q_3 = m_\mu^2/6 - m_e^2/2$ and $\sigma_0(\mu \rightarrow \nu_\mu e^- \bar{\nu}_e)$ is the tree-level cross section.

from Eqs.(13,26) and Eq.(29) we find this gauge dependence doesn't appear in the result of the pole mass renormalization prescription.

IV. CONCLUSION

Through calculating the singularities of W and Z's two-loop-level transverse self energy we find the counterterms of W and Z's mass and the sine of the weak mixing angle are gauge dependent under the on-shell mass renormalization prescription. The gauge dependencies of these counterterms lead to the cross section of $\mu \rightarrow \nu_\mu e^- \bar{\nu}_e$ gauge dependent at two-loop level. So the on-shell mass renormalization prescription is a wrong mass renormalization prescription beyond one-loop level.

On the other hand, all of the above gauge dependencies don't appear in the results of the pole mass renormalization prescription. So the pole mass renormalization prescription is the only reasonable candidate for the mass renormalization prescription at present. We should use the pole mass renormalization prescription rather than the on-shell mass renormalization prescription to calculate physical results beyond one-loop level.

Acknowledgments

The author thanks Prof. Xiao-Yuan Li and Prof. Cai-dian Lu for their useful guidance.

[1] M. Veltman, *Physica* **29** (1963) 186;
 D. Bardin and G. Passarino, *The Standard Model in the Making Precision Study of the Electroweak Interactions*, Oxford Science Pub., Clarendon Press, Oxford,1999.

[2] A. Denner, *Fortschr. Phys.* **41** (1993) 307.

[3] A. Sirlin, *Phys. Rev. Lett.* **67** (1991) 2127; *Phys. Lett. B* **267** (1991) 240;
 R.G. Stuart, *Phys. Lett. B* **272** (1991) 353.

[4] M. Passera, A. Sirlin, *Phys. Rev. Lett.* **77** (1996) 4146;
 B.A. Kniehl, A. Sirlin, *Phys. Rev. Lett.* **81** (1998) 1373;
 P.A. Grassi, B.A. Kniehl and A. Sirlin, *Phys. Rev. Lett.* **86** (2001) 389;
 M.L. Nekrasov, *Phys. Lett. B* **531** (2002) 225;
 B.A. Kniehl, A. Sirlin, *Phys. Lett. B* **530** (2002) 129;

[5] J.C. Breckenridge, M.J. Lavelle, T.G. Steele, *Z. Phys. C* **65** (1995) 155.

[6] P. Gambino, P.A. Grassi, *Phys. Rev. D* **62** (2000) 076002 (hep-ph/9907254).

[7] N.K. Nielsen, *Nucl. Phys. B* **101** (1975) 173;
 R. Tarrach, *Nucl. Phys. B* **183** (1981) 384;
 O. Piguet and K. Sibold, *Nucl. Phys. B* **253** (1985) 517;
 N. Gray, D.J. Broadhurst, W. Grafe, K. Schilcher, *Z. Phys. C* **48** (1990) 673;
 D.J. Broadhurst, N. Gray, K. Schilcher, *Z. Phys. C* **52** (1991) 111.

[8] J. Kublbeck, M. Bohm, A. Denner, *Comput. Phys. Commun.* **60** (1990) 165;
 G.J. van Oldenborgh, J.A.M. Vermaasen, *Z. Phys. C* **46** (1990) 425;
 T. Hahn, M. Perez-Victoria, *Comput. Phys. Commun.* **118** (1999) 153.

[9] J. Gegelia, G. Japaridze, A. Tkabladze, A. Khelashvili, K. Turashvili, hep-ph/9910527;
 F. Jegerlehner, M.Yu. Kalmykov and O. Veretin, *Nucl. Phys. B* **641** (2002) 285;
 F. Jegerlehner, M.Yu. Kalmykov and O. Veretin, *Nucl. Phys. B* **658** (2003) 49.

[10] A. Freitas, W. Hollik, W. Walter, G. Weiglein, *Phys. Lett. B* **495** (2000) 338;
 A. Freitas, W. Hollik, W. Walter, G. Weiglein, *Nucl. Phys. B* **632** (2002) 189.

[11] N. Cabibbo, *Phys. Rev. Lett.* **10**, 531 (1963);
 M. Kobayashi and K. Maskawa, *Prog. Theor. Phys.* **49** (1973) 652.

[12] R.E. Cutkosky, *J. Math. Phys.* **1**, 429 (1960);
 Yong Zhou, hep-ph/0508225.

[13] The European Physical Journal C, 15 (2000) 1-878.